Decoding cancer metabolism: A pan-cancer proteomics perspective

Yiguang Bai[1,2#*] Qiaoling Chen[3,4#] Yuan Li[5,6*]

[1]Department of Orthopedics, Beijing Anzhen Nanchong Hospital, Capital Medical University (Nanchong Central Hospital), Nanchong, China

[2]Department of Orthopedics, Nanchong Central Hospital, The Second Clinical Medical College of North Sichuan Medical College, Nanchong, China

[3]Department of Oncology, Beijing Anzhen Nanchong Hospital, Capital Medical University (Nanchong Central Hospital), Nanchong, China

[4]Department of Oncology, Nanchong Central Hospital, The Second Clinical Medical College of North Sichuan Medical College, Nanchong, China

[5]Department of Immunotechnology, Lund University, Medicon Village, Lund, 22387, Sweden

[6]National Bioinformatics Infrastructure Sweden (NBIS), Science for Life Laboratory, Lund University, Lund, 223 87, Sweden

[#]Those authors contribute equally to the paper.

[*]Corresponding author: yuan.li@immun.lth.se, baiyiguang@163.com

Abstract

Metabolic reprogramming is a hallmark of cancer, yet the extent to which metabolic alterations are shared or distinct across cancer types remains incompletely understood. Here, we performed a systematic reanalysis of large-scale proteomic datasets spanning 16 diverse human cancers to uncover global and tissue-specific patterns of metabolic dysregulation. We

found a striking inverse correlation between baseline metabolic activity in matched normal tissues and the degree of metabolic rewiring in tumors, pointing to a context-dependent metabolic shift during oncogenesis. Our analysis reveals frequently upregulated glycosylation-related pathways across cancers, along with coordinated alterations in nucleotide, carbohydrate, amino acid, and coenzyme & cofactor metabolism that collectively support biosynthesis, maintain redox balance, and sustain oncogenic signaling. These changes enable cancer cells to proliferate rapidly, evade cell death, and adapt to fluctuating environmental conditions. Together, our findings delineate both conserved and lineage-specific features of tumor metabolism, providing a pan-cancer perspective that may aid in identifying selective metabolic vulnerabilities and guiding the development of targeted therapeutic strategies.

Keywords

Cancer, Metabolism, Proteomics, Glycosylation, Pan-cancer

Introduction

Cancer cells undergo profound metabolic reprogramming to sustain rapid proliferation, resist cell death, and adapt to fluctuating environmental conditions [1, 2]. Unlike normal cells, which primarily metabolize nutrients to maintain homeostasis, cancer cells remodel their metabolism to meet the biosynthetic, energetic, and redox demands of tumor growth and progression [3, 4]. This reprogramming is now recognized as a hallmark of cancer, reflecting both the consequences and drivers of oncogenic signaling [5].

A central feature of this metabolic shift is the Warburg effect, whereby cancer cells preferentially use aerobic glycolysis and produce lactate even in the presence of oxygen [6, 7]. This pathway not only allows for rapid Adenosine triphosphate (ATP) generation but also

provides glycolytic intermediates for the biosynthesis of nucleotides, amino acids, and lipids [2, 4]. However, mitochondrial metabolism is not abandoned; rather, the tricarboxylic acid (TCA) cycle remains active and is often reprogrammed to function as a biosynthetic hub [1]. It integrates nutrients such as glucose, glutamine, and fatty acids to support anabolic growth and maintain metabolic flexibility [1, 8, 9]. The TCA cycle also supplies reducing equivalents (NADH, FADH□) to drive oxidative phosphorylation, further contributing to energy production. This dual engagement of glycolysis and oxidative metabolism enables cancer cells to thrive in nutrient- and oxygen-variable microenvironments [10].

To cope with heightened metabolic flux and oxidative stress, cancer cells engage in sophisticated redox regulation by elevating Nicotinamide adenine dinucleotide phosphate (NADPH) production through multiple pathways. These include the oxidative pentose phosphate pathway (PPP), malic enzyme (ME1/2), and cytosolic/mitochondrial isocitrate dehydrogenases (IDH1/2), collectively sustaining antioxidant systems such as glutathione and thioredoxin [1, 2]. Mitochondrial metabolism plays a dual role—serving as a major site of reactive oxygen species (ROS) generation while also contributing to redox buffering via modulation of NADH/NAD□ equilibria [1, 2]. This fine-tuned redox balance supports not only survival but also therapeutic resistance and immune evasion [1, 2].

Importantly, cancer cells extend their metabolic influence to the tumor microenvironment. They scavenge nutrients from the extracellular matrix and manipulate stromal cell metabolism to generate a supportive niche [2, 11]. Hypoxia—a common feature of solid tumors—stabilizes hypoxia-inducible factors (HIFs), which rewire metabolism to favor glycolysis and angiogenesis, further promoting tumor adaptation and growth [2, 12]. Additionally, altered glycan metabolism modifies cell–cell and cell–matrix interactions, facilitates immune escape, and promotes metastasis [13, 14]. Cancer cells also compete with

immune cells for critical nutrients such as glucose and tryptophan, and release immunosuppressive metabolites like lactate and kynurenine that suppress anti-tumor immunity [2, 15].

Cancer metabolism also plays a pivotal role in shaping the epigenetic landscape of both tumor and surrounding cells. Many epigenetic enzymes require metabolic intermediates as cofactors or substrates—for example, acetyl coenzyme A (acetyl-CoA) for histone acetylation, and S-adenosylmethionine (SAM) for methylation reactions [2]. Mutations in metabolic enzymes such as IDH1/2, succinate dehydrogenase, or fumarate hydratase can lead to the accumulation of oncometabolites like 2-hydroxyglutarate, succinate, and fumarate, which inhibit α-ketoglutarate–dependent dioxygenases and result in aberrant deoxyribonucleic acid (DNA) and histone methylation [2]. These epigenetic alterations block differentiation and promote tumorigenesis [2]. Moreover, metabolic crosstalk affects non-cancerous cells in the microenvironment: secreted oncometabolites and nutrient competition can disrupt the epigenetic programming of stromal and immune cells, converting them into pro-tumor phenotypes or suppressing their anti-tumor functions [16, 17]. Hypoxia further amplifies this effect by inhibiting oxygen-dependent epigenetic modifiers and creating a chromatin state conducive to tumor progression [18, 19].

Advancing our understanding of cancer metabolism demands comprehensive pan-cancer approaches that capture both common and context-specific metabolic adaptations across diverse tumor types [3, 20-22]. Computational tools like CellFie [23], which infer metabolic task activities from transcriptomic or proteomic data, enable systematic and scalable profiling of metabolic rewiring across large cancer cohorts. By integrating omics data with curated genome-scale metabolic models, CellFie quantifies task-level activities within individual tumors, revealing shifts in nutrient utilization, redox balance, biosynthesis, and other critical

metabolic functions [23]. Applying CellFie to pan-cancer datasets uncovers conserved metabolic programs, cancer-type–specific vulnerabilities, and tissue-dependent rewiring events often undetectable by metabolite-level analyses. This strategy enhances mechanistic insights into how metabolic plasticity supports tumor progression and exposes novel therapeutic targets—including essential metabolic tasks and compensatory pathways—tailored to tumor subtype, stage, or microenvironmental context. Here, we apply CellFie to large-scale proteomic datasets from 16 distinct cancer types (including 2,447 samples) to systematically characterize metabolic rewiring, paving the way for identifying new therapeutic vulnerabilities and advancing precision oncology.

Methods

Proteomics dataset for 16 cancer types

We assembled a comprehensive compendium of Mass Spectrometry (MS)-based proteomics data comprising 16 different cancer types, encompassing 2,447 samples from 1,440 patients, collected from thirteen independent studies (Table S1, Table S2). The dataset includes both tumor and matched non-tumor samples for each cancer type, as follows: breast invasive ductal carcinoma (BRCA; cancer, n = 5; non-cancer, n = 5; [24]), colon adenocarcinoma (COAD; cancer, n = 108; non-cancer, n = 111; [24, 25]), esophageal squamous cell carcinoma (ESCC; cancer, n = 131; non-cancer, n = 130; [24, 26]), glioblastoma (GBM; cancer, n = 111; non-cancer, n = 10; [24, 27]), head and neck squamous cell carcinoma (HNSC; cancer, n = 114; non-cancer, n = 68; [24, 28]), kidney renal clear cell carcinoma (KIRC; cancer, n = 101; non-cancer, n = 94; [24, 29]), liver hepatocellular carcinoma (LIHC; cancer, n = 173; non-cancer, n = 173; [24, 30]), lung adenocarcinoma (LUAD; cancer, n = 119; non-cancer, n = 109; [24, 31]), lung squamous cell carcinoma (LUSC; cancer, n = 116; non-cancer, n = 107; [24, 32]), ovarian serous cystadenocarcinoma (OV; cancer, n = 90; non-

cancer, *n* = 26; [24, 33]), pancreatic adenocarcinoma (PAAD; cancer, *n* = 148; non-cancer, *n* = 72; [24, 34]), stomach adenocarcinoma (STAD; cancer, *n* = 88; non-cancer, *n* = 87; [24, 35]), uterine corpus endometrial carcinoma (UCEC; cancer, *n* = 74; non-cancer, *n* = 29; [24, 36]), bladder invasive urothelial carcinoma (BLCA; cancer, *n* = 11; non-cancer, *n* = 11; [24]), prostate adenocarcinoma (PRAD; cancer, *n* = 7; non-cancer, *n* = 7; [24]), and lung small cell carcinoma (SCLC; cancer, *n* = 6; non-cancer, *n* = 6; [24]).

Within these datasets, Zhou et al. (2020) [24] generated a dataset, which covers all 16 cancer types (8–22 samples per type; Fig. 1A) and exhibits relatively small batch effects between cancer types. This subset will hereafter be referred to as the Zhou2020 dataset. In total, 7,725 proteins were analyzed in the Zhou2020 dataset. The dataset had already been preprocessed by Zhou et al. (2020) [24]. Briefly, raw data acquired using data-independent acquisition (DIA) MS were quantified and normalized with Spectronaut Pulsar X. Proteins were filtered using a Q-value cutoff of 0.01 (corresponding to a 1% false discovery rate, FDR), retaining only those quantified in at least 40% of samples within each cancer type. Missing values were imputed. The processed protein abundance matrix, together with sample annotations, was obtained from the published study.

Figure 1

For the other datasets—covering twelve different cancer types (95–330 samples per type; Figure 1B) from twelve independent studies (Table S1)—we analyzed them together, yielding a total of 1,862 proteins. These datasets were compiled and reprocessed by Hu et al. (2025) [37]. In brief, Hu et al. (2025) [37] downloaded raw MS files from either the Clinical Proteomic Tumor Analysis Consortium (CPTAC) [38] or Proteomics IDentifications Exchange (PRIDE), and analyzed them using MaxQuant v2.0.2.0. The resulting protein abundances were log□-transformed and normalized using median-

centering across proteins. The processed data and sample annotations were obtained from either the Cancer Proteome and Phosphoproteome Atlas (CPPA) or the corresponding published studies. Only batches containing both normal and tumor samples were included in the analysis. These datasets will hereafter be referred to as the Hu2025-harmonized datasets or the other datasets.

Metabolic task scoring using CellFie

To enable phenotype-relevant interpretation of the extensive proteomics data across 16 cancer types, we grouped the detected proteins into distinct metabolic tasks and quantified the activity of each task based on protein abundance using CellFie on the GenePattern webserver [23]. In metabolism, metabolic tasks are defined as small modules of reactions that convert specific substrate metabolites into defined product metabolites [23]. The ability to regulate these tasks allows cancer cells to reprogram their metabolism, thereby supporting rapid growth, survival, invasion, and resistance to therapy [1, 2].

All proteins were mapped to Entrez Gene IDs prior to submission using the annotation package org.Hs.eg.db v3.20.0 with the select() function from AnnotationDbi v1.68.0. The Zhou2020 dataset was log□-transformed before submission, whereas the other datasets underwent an exponential transformation with base 2 to avoid negative values.

We applied a local thresholding approach (feature-specific thresholding with Local.Threshold.Type = "minmaxmean") to classify features as “active” or “inactive” based on their abundance. For each feature, the threshold was defined as the mean expression value across all samples, constrained by two bounds: it had to be at least as high as the 25th percentile (lower bound) and no higher than the 75th percentile (upper bound) of the overall protein abundance distribution across the dataset.

CellFie also provides binary task scores indicating whether a metabolic task is active or inactive, based on the expression profiles of their constituent features. All Zhou2020 samples were submitted to CellFie together in a single file, while datasets from the other studies were submitted individually to the GenePattern webserver.

Metabolic activities at higher organizational levels: subsystems (Depth 2) and systems (Depth 1)

To facilitate interpretation of the metabolic task scores generated by CellFie, we aggregated the individual task scores or binary task scores within broader metabolic categories (subsystems or systems) by averaging them. This produced single values—mean task scores or percentages of active tasks—for each subsystem or system in every sample.

Differential analysis of metabolic activities between Cancer and Normal samples

To understand how cancer cells reprogram their metabolic processes to support rapid growth, survival, invasion, and therapy resistance, we performed univariate differential analysis using linear models implemented in limma v3.62.2 [39]. Each metabolic task was tested individually for differences between tumor and matched normal samples.

In this analysis, the Zhou2020 dataset was analyzed separately from Hu2025-harmonized datasets. Due to the larger sample sizes of those Hu2025-harmonized datasets (Fig. 1B), the differential analysis results from these datasets are expected to be more robust.

Differential analysis could not be performed for GBM in the Zhou2020 dataset due to the absence of matched normal samples. For BLCA, BRCA, COAD, ESCC, HNSC, KIRC, LIHC, LUAD, SCLC, LUSC, PAAD, STAD, and UCEC, paired differential analysis was conducted with the help of the duplicateCorrelation() function in limma v.3.62.2. For PRAD and OV, where insufficient paired samples were available, standard differential analysis was

performed. In all analyses, only metabolic tasks with at least two quantified scores in each sample group (normal and tumor) were included.

For the twelve cancer types in the Hu2025-harmonized datasets, the duplicateCorrelation() function from limma v3.62.2 was used to account for the correlation between paired samples from the same patients, while also controlling for batch effects when multiple batches were present within a single cancer type.

Benjamini-Hochberg correction was applied to control the false discovery rate. Differential analysis was conducted not only at the level of individual metabolic tasks but also at the broader subsystem and system levels. Tasks, subsystems, or systems with an adjusted p-value (p.adj) less than 0.05 were considered statistically significant.

Correlation between normal tissue metabolic activity and task differential log fold change

For each cancer type, we calculated Pearson correlation coefficients across all identified metabolic tasks between the baseline percentages of active metabolic tasks in matched normal tissues and the log fold change (logFC) of task scores comparing tumor to normal tissues. This analysis aimed to determine whether baseline metabolic activity is associated with metabolic rewiring. Correlations were computed using the cor.test() function in R v4.4.3, and Benjamini-Hochberg correction was applied to control the false discovery rate. These analyses were conducted separately for the Zhou2020 dataset and the datasets harmonized by Hu et al. (2025)[37].

Data visualization

Data visualization was performed using R v4.4.3. Circular barplots, dotplots, barplots and volcano plots were created with ggplot2 v3.5.2. Circular packing plots were generated using ggraph v2.2.1, while upset plots were produced with ComplexHeatmap v2.22.0.

Results

Metabolic activity varies across both cancer types and metabolic systems

To investigate pan-cancer metabolic reprogramming, we compiled a comprehensive dataset of MS-based proteomics, encompassing 16 different cancer types, 2,447 samples, and 1,440 patients, collected from thirteen independent studies (Table S1, Table S2). Within this dataset, the data from Zhou et al. (2020) [24], which cover all 16 cancer types (Fig. 1A) and exhibit minimal batch effects across cancer types, were analyzed collectively. The other datasets, compiled and harmonized by Hu et al. (2025) [37], include twelve cancer types (Fig. 1B) from twelve separate studies (Table S1) and were analyzed together as well. To enable phenotype-relevant interpretation of the extensive proteomics data across these cancer types, we categorized the detected proteins into distinct metabolic tasks and quantified their activities based on protein abundance using CellFie [23].

In total, we identified 176 active metabolic tasks (Depth 3) in the Zhou2020 dataset. These tasks were grouped into 68 metabolic subsystems (Depth 2), which were further organized into seven systems (Depth 1): energy, nucleotide, carbohydrate, amino acid, lipid, vitamin & cofactor, and glycan metabolism (Fig. 1C, Table S3). In the other datasets, we identified 138 active metabolic tasks, grouped into 58 metabolic subsystems and the same seven systems (Fig. 1D, Table S3).

Among the 16 cancer types in the Zhou2020 dataset, LIHC exhibits the highest percentage of active metabolic tasks (90%) in both normal and tumor tissues (Fig. 2A, TableS4). This is

followed by KIRC, STAD, and PAAD, each with over 80% active tasks in normal tissues, and by GBM, STAD, and PRAD, each with over 80% in tumor tissues. The percentage of active tasks then gradually decreases to about 37% in normal tissues and 64% in tumors (Fig. 2A & B, Table S4), suggesting that metabolic task activity increases in cancers with lower baseline metabolic activity in normal tissues. When analyzed by the seven broad metabolic systems, STAD and LIHC rank among the top three for six of the seven systems in normal and tumor tissues, respectively (Fig. 2A & B, Table S4). Additionally, both LIHC and KIRC rank among the top three in five of the seven systems in normal tissues (Fig. 2A & B, Table S4).

Figure 2

In contrast, the percentage of active metabolic tasks in the Hu2025-harmonized datasets is considerably lower, with all cancer types below 70% except for STAD (in both normal and tumor tissues) and GBM (in normal tissue). The majority of cancer types in these datasets show around 50% or lower activity, which may reflect the smaller number of proteins analyzed (n = 1,862) in these datasets (Fig. 3A & B, Table S4). When broken down to metabolic system level, STAD ranks among top three in both normal and tumor tissues in all systems except glycan metabolism, where all cancer types show low activities (<56%) (Fig. 3A&B, Table S4).

Figure 3

Among the seven metabolic systems studied (Depth1), carbohydrate and lipid metabolism exhibit the highest activity levels in matched normal tissues from both the Zhou2020 and the Hu2025-harmonized datasets, followed by energy, amino acid, and nucleotide metabolism. Glycan metabolism shows the lowest activity in normal tissues, with vitamin & cofactor metabolism being the next least active (Fig. 2A & B, Fig. 3A & B, Table S4). Compared to

normal tissues, the activities of all metabolic systems appear generally increased in tumor tissues, with especially pronounced elevations in glycan metabolism and vitamin & cofactor metabolism (Fig. 2A & B, Fig. 3A & B, Table S4). This trend is particularly evident in cancer types with lower baseline metabolic activity (Fig. 2A & B, Fig. 3A & B, Table S4).

Cancer metabolic rewiring varies across cancer types

At the metabolic task level (Depth3), among the twelve cancer types harmonized by Hu et al. (2025) [37], between three and 107 metabolic tasks were found to be upregulated, with LUAD showing the highest number (n = 107), followed by LUSC, ESCC, and KIRC (each with more than 55) (Fig. S1, Table S5). Conversely, five to 116 tasks were identified as downregulated, with PAAD having the most (n = 116), followed by LIHC, STAD, COAD, HNSC, and GBM (each with over 70) (Fig. S1, Table S5). For the 15 compared cancer types from the Zhou2020 dataset, zero to 75 tasks were upregulated, with SCLC showing the highest count (n = 75), while the others had fewer than 40 (Fig. S1, Table S5). In contrast, zero to 109 tasks were downregulated, with KIRC having the most (n=109), followed by STAD (n = 84) and LIHC (n = 55), and the remaining cancer types having fewer than 35 (Fig. S1, Table S5).

At the metabolic subsystem level (Depth2), among the twelve cancer types harmonized by Hu et al. (2025) [37], between one and 43 subsystems were found to be upregulated, with LUAD and LUSC showing the highest numbers (43 and 41, respectively), followed by ESCC and KIRC (each with more than 25) (Fig. S2, Table S5). Conversely, one to 49 subsystems were identified as downregulated, with PAAD having the most (n = 49), followed by STAD, LIHC, COAD, HNSC, and GBM (each with over 25) (Fig. S2, Table S5).

For the 15 compared cancer types from the Zhou2020 dataset, zero to 31 subsystems were upregulated, with SCLC showing the highest count (n = 31), followed by BLCA (n = 21),

while the others had fewer than 20 (Fig. S2, Table S5). In contrast, 0 to 41 subsystems were downregulated, with KIRC having the most (n=41), followed by STAD (n = 26), LIHC (n = 19), and BRCA (n=17), and the remaining cancer types below ten (Fig. S2, Table S5).

At the metabolic system level (Depth1), among the twelve cancer types harmonized by Hu et al. (2025), between zero and six systems were identified as upregulated. LUAD and ESCC exhibited the highest numbers (six each), followed by LUSC and KIRC (five each) (Fig. S3, Table S5). Conversely, zero to seven systems were found to be downregulated, with PAAD showing the most (n = 7), followed by STAD (n = 6), LIHC (n = 5), and COAD (n = 4) (Fig. S3, Table S5). For the 15 compared cancer types in the Zhou2020 dataset, between zero and four systems were upregulated, with SCLC having the most (n = 4), followed by UCEC (n = 3), while the rest had two or fewer (Fig. S3, Table S5). In contrast, zero to six systems were downregulated, with KIRC showing the highest count (n = 6), followed by LIHC (n = 3), and the remainder having two or fewer (Fig. S3, Table S5).

Overall, the twelve cancer datasets harmonized by Hu et al. (2025) [37] share more common up- and downregulated tasks compared to those acquired by Zhou et al. (2020) [24] (Figs. S1, S2, & S3), which may be because of the larger sample sizes in the Hu2025-harmonized datasets (Fig. 1).

Additionally, among the twelve cancer types harmonized by Hu et al. (2025) [37], LUAD, LUSC, ESCC, KIRC, UCEC, and OV tend to exhibit more upregulated metabolic tasks, subsystems, and systems than downregulated ones, whereas PAAD, STAD, LIHC, COAD, HNSC, and GBM show the opposite trend with more downregulated features (Fig. 3C, Fig. S4A). Similar patterns were observed in the 15 compared cancer types acquired by Zhou et al. (2020) [24]: LUAD, LUSC, UCEC, OV, SCLC, and BLCA generally have more upregulated

tasks, subsystems, and systems, while STAD, LIHC, and KIRC tend to have more downregulated ones (Fig. 2C, Fig. S4B).

Cancer metabolic rewiring varies across metabolic categories

Despite the large number of dysregulated metabolic tasks identified, we found no single metabolic task that was consistently dysregulated across all studied cancer types, including those in the large Hu2025-harmonized datasets (Fig. S5, Fig. S6). However, many glycan metabolic tasks, nucleotide metabolic tasks, and glycosylation-related carbohydrate metabolic tasks in the Hu2025-harmonized datasets are widely upregulated, occurring in six or more cancer types (Fig. S5). In contrast, most lipid metabolic tasks tend to be downregulated (Fig. S5). Furthermore, the most frequently upregulated tasks (observed in eight or more cancer types) are primarily related to glycosylation processes, including: biosynthesis of m4mpdol_U (a specific glycan intermediate involved in N-glycan biosynthesis in the cytosol), keratan sulfate biosynthesis from N-glycan, keratan sulfate biosynthesis from O-glycan (core 2- and core 4-linked), UDP-N-acetyl D-galactosamine synthesis, lactose synthesis, CMP-N-acetylneuraminate synthesis, GDP-L-fucose synthesis, and N-acetylglucosamine synthesis (Fig. 4B). The last three top upregulated tasks involve essential coenzyme and amino acid metabolism, including NAD synthesis from nicotinamide and the conversions of glutamate to glutamine and proline (Fig. 4B). No metabolic task was consistently dysregulated in eight or more cancer types within the Zhou2020 dataset (Fig. S6). However, the two most frequently upregulated tasks—observed in seven cancer types—are also glycosylation-related: glucosaminyl−acylphosphatidylinositol to deacylated−glycophosphatidylinositol (GPI)-anchored protein, and GDP-L-fucose synthesis (Fig. 5B).

Similar patterns were observed at the subsystem level (Depth2), where the top upregulated subsystems in eight or more cancer types are glycosylation-related metabolisms, including

amino sugar metabolism, keratan sulfate metabolism, galactose metabolism, N-glycan metabolism, and fucose metabolism, along with coenzyme NAD biosynthesis in the Hu2025-harmonized dataset (Fig. 4A). In the Zhou2020 dataset, no subsystem was consistently dysregulated in eight or more cancer types, but the top two regulated subsystems—amino sugar and fucose metabolism—were upregulated in seven cancer types (Fig. 5A). At the system level (Depth1), the top upregualted systems are glycan metabolism and vitamin & cofactor metabolism in both the Zhou2020 and Hu2025-harmonized datasets (Figs. 4C & 5C).

Figure 4

Figure 5

Metabolic reprogramming as an inverse response to baseline activity in normal tissues

From the results above, we observed that cell types with more upregulated tasks than downregulated tasks tend to have lower baseline active task percentages in normal tissues. Conversely, those with more downregulated tasks than upregulated tasks tend to exhibit higher baseline active task percentages in normal tissues (Fig. 2A & C, Fig. 3A & C).

To investigate this further, we calculated the correlation coefficients between the logFC of metabolic task scores in tumor versus matched normal tissues and the active task percentages in the matched normal tissues, considering all identified tasks. This analysis was performed separately for each cancer type.

The results show that these correlations are negative across all cancer types, and they are statistically significant in most cases (adjusted p-value < 0.05) (Fig. 2D, Fig. 3D, Table S6).

Discussion

In this study, we conducted a systematic reanalysis of proteomic data from 16 distinct cancer types across multiple studies to characterize patterns of metabolic reprogramming in cancer. Our findings reveal both cancer-type-specific and shared alterations in metabolic pathways, including an inverse relationship between baseline activities in normal tissues and cancer-associated metabolic rewiring, frequent upregulation of glycosylation-related metabolism, and adaptive regulation of nucleotide, coenzyme, carbohydrate, and amino acid metabolic activities to modulate oncogenic signaling, supply building blocks and cellular energy, and mitigate ROS stress. These results underscore the complexity and heterogeneity of cancer metabolism, suggesting that while some metabolic features are conserved across most cancers, others reflect lineage-dependent adaptations. This pan-cancer perspective advances our understanding of tumor-specific metabolic vulnerabilities and may inform the development of more tailored therapeutic strategies.

Cancer metabolic rewiring dynamics inversely related to baseline activity in normal tissue

It is well established that each normal tissue has evolved specialized metabolic programs to support its unique functions, while simultaneously maintaining certain pathways at low activity to preserve homeostasis and avoid unnecessary energy expenditure or biosynthesis. This is reflected in our observations of metabolism in matched normal tissues, which show great variability in tissue-specific activities. For example, STAD exhibits very high activity across nearly all metabolic systems, whereas LUAD, LUSC, UCEC, and OV generally display low metabolic activities. This pattern holds true both in the Zhou2020 dataset and in other datasets (Figs. 2A, 3A).

Moreover, baseline activities vary considerably among different metabolic systems. For instance, glycan, vitamin & cofactor metabolism tend to have low activity in most normal

tissues, while carbohydrate, lipid, and energy metabolism are highly active in most normal tissues (Figs. 2A, 3A).

Compared to normal tissues, metabolic activities are generally elevated in cancer, particularly in glycan metabolism, vitamin & cofactor metabolism, and in cancer types that typically have lower baseline activity (Fig. 2A & B, Fig. 3A & B, Table S4).

To explore this further, we calculated the correlation coefficients between the active task percentages across all normal samples and the logFC of task scores between tumor and normal tissues. These correlations were significantly negative in most cancers, suggesting that cancer metabolic rewiring may be inversely related to baseline activity in normal tissues (Fig. 2D, Fig. 3D).

Tumorigenesis exhibits tissue-specific differences [22], and that cancer cells have metabolic requirements that vary depending on tissue and context [3, 40, 41]. Our findings suggest that these tissue-specific metabolic rewiring events in cancer are largely driven by cancer cells' attempts to compensate for the limited metabolic capabilities of their tissue of origin. While normal tissues maintain tightly regulated and specialized metabolic programs, tumor cells reprogram these pathways to fulfill the heightened demands of proliferation, survival, and stress resistance. This metabolic compensation enables cancer cells to overcome lineage-imposed constraints by activating suppressed or alternative pathways, thereby supporting rapid growth and adaptation across diverse tissue types.

Frequently upregualted glycosylation-related metabolism in cancer

Glycosylation, the addition of glycans to molecules such as proteins, plays a crucial role in malignant transformation and cancer metastasis [44]. Aberrant glycosylation in cancer contributes to various processes, including cell signaling and communication, tumor cell

dissociation and invasion, cell–matrix interactions, tumor angiogenesis, immune modulation, and metastasis formation [13, 14, 44]. Glycans, amino sugars, and fucose are interconnected components of the cellular glycosylation machinery.

In the present study, one of the most notable findings is the generally low baseline activity of glycan metabolism, followed by a dramatic upregulation in the twelve cancer types harmonized by Hu et al. (2025) [37] (Figs. 3A&B, S5, S7, S9). Furthermore, amino sugar metabolism—which includes CMP-N-acetylneuraminate synthesis, UDP-N-acetyl D-galactosamine synthesis, and N-acetylglucosamine synthesis—and fucose metabolism (GDP-L-fucose synthesis) were significantly upregulated in nine and eight of these cancer types, respectively (Fig. 4A).

These results collectively suggest that alterations in glycosylation represent important biomarkers and offer a promising set of specific targets for therapeutic intervention [42, 43].

Rewired nucleotide and amino acid metabolic pathways promote anabolic growth in cancer

The rapid proliferation of cancer cells places a high demand on building materials and cellular energy. To meet these demands, cancer cells often reprogram their metabolic activities [1, 4]. Biosynthetic, or anabolic, pathways are a critical component of cancer metabolism, as they enable cells to produce the macromolecules necessary for cell division and tumor growth. The three main macromolecular classes studied in cancer metabolism are proteins, lipids, and nucleic acids, which constitute approximately 60%, 15%, and 5% of the dry mass of mammalian cells, respectively [1]. Evidence suggests that the biosynthesis of all three macromolecule classes is regulated by the same signaling pathways that control cell growth. These pathways, particularly the PI3K-mTOR axis, are frequently activated in cancer due to tumorigenic mutations [1].

Nucleotide metabolism encompasses the synthesis, salvage, and degradation of purine and pyrimidine nucleotides—the essential building blocks of DNA and ribonucleic acid (RNA) [45]. Enhanced nucleotide metabolism is a critical and universal metabolic dependency of cancer cells across various cancer types and genetic backgrounds [20]. Many aggressive cancer behaviors, including uncontrolled proliferation, chemotherapy resistance, immune evasion, and metastasis, heavily rely on this upregulated nucleotide metabolism [20]. Consistent with these earlier findings, we observed a clear overall increase in nucleotide metabolism in cancer compared to normal tissues in both the Zhou2020 and Hu2025-harmonized datasets (Figs. 2 & 3). This increase was statistically significant in six of the twelve cancer types from the Hu2025-harmonized dataset: COAD, ESCC, GBM, KIRC, LIHC, and LUSC (Fig. 4C).

Protein biosynthesis is tightly regulated and requires a complete supply of both essential and nonessential amino acids [1]. Additionally, amino acids serve as precursors for the synthesis of nucleotides and lipids [46, 47]. In the present study, we found that overall amino acid metabolic activity was upregulated in only four cancer types (ESCC, UCEC, LUAD, LUSC) but downregulated in six (COAD, GBM, HNSC, LIHC, PAAD, and STAD) among the twelve cancers harmonized by Hu et al. (2025) [37] (Fig. 4C). Notably, most of the downregulated pathways shared by at least six cancer types involve amino acid degradation (Fig. S5). In the 16 cancers acquired by Zhou et al. (2020) [24], only UCEC exhibited upregulated amino acid metabolism (Fig. 5C). These patterns inversely reflect the metabolic activities observed in matched normal tissues (Figs. 2A & 3A), suggesting that baseline amino acid metabolism is generally robust in normal tissues and primarily maintained by reducing degradation in cancer.

Cancer cells frequently develop dependencies on specific amino acids, reflecting their reliance on altered metabolic fluxes to support rapid growth and survival. In our analysis of the twelve cancer types harmonized by Hu et al. (2025) [37], several amino acid metabolic pathways were upregulated in at least half of the cancers, including the conversion of glutamate to glutamine, conversion of glutamate to proline, glycine synthesis, serine synthesis, and spermidine synthesis from ornithine (Fig. S5).

The conversion of glutamate to glutamine, catalyzed by glutamine synthetase and upregulated in eight cancers, plays a central role in cancer metabolism, particularly in tumors facing glutamine scarcity or altered nitrogen homeostasis. Glutamine, the most abundant plasma amino acid, fuels nucleotide, amino acid, and lipid biosynthesis and is often the most rapidly consumed nutrient in tumor cells—a phenomenon termed “glutamine addiction” [46, 48, 49]. This amino acid frequently functions as a rate-limiting factor for cell cycle progression, with glutamine deprivation causing arrest in the S-phase [46, 50].

Similarly, the conversion of glutamate to proline is emerging as a key metabolic adaptation in cancer, supporting both anabolic demands and stress resilience. Although proline is classified as a non-essential amino acid, rapidly proliferating cancer cells require elevated proline levels for collagen synthesis—the principal component of the extracellular matrix—which upon degradation supplies essential substrates and energy to the tumor microenvironment, as well as for general protein biosynthesis [46].

Glycine, the simplest amino acid, is critical for supporting rapid proliferation, stress adaptation, and the biosynthesis of vital macromolecules including proteins and nucleotides [46]. Likewise, serine synthesis plays a pivotal role in cancer metabolism, intricately linked to proliferation, redox homeostasis, nucleotide synthesis, and epigenetic regulation [46].

Furthermore, spermidine—a key polyamine derived from ornithine—is implicated in numerous fundamental cellular processes such as nucleic acid and protein synthesis, chromatin structure stabilization, differentiation, apoptosis, protection against oxidative damage, and regulation of ion channels essential for intercellular communication [51]. Dysregulation of polyamine metabolism is a hallmark of cancer, with elevated polyamine levels frequently promoting tumor progression and cellular transformation [51].

Collectively, these findings underscore the critical role of specific amino acid metabolic pathways in supporting cancer cell growth and survival, highlighting potential metabolic vulnerabilities for therapeutic intervention.

Lipid metabolism is frequently suppressed in cancer

In contrast to nucleotide metabolism, lipid metabolic activities are predominantly downregulated in most cancers in the Hu2025-harmonized datasets (Figs. 4A & S5). This is not surprising, given the relatively high baseline levels of lipid metabolism observed in the matched normal tissues (Fig. 3A), which may already provide more than sufficient structural components for biological membranes to support the rapid proliferation of cancer cells.

Altered carbohydrate and energy metabolism fuel anabolic growth by supplying building blocks and ATP in cancer

In cancer, carbohydrate metabolism is extensively reprogrammed to support rapid proliferation, survival, and adaptation to environmental stresses [1, 2]. A hallmark of this metabolic reprogramming is the Warburg effect, wherein cancer cells preferentially utilize aerobic glycolysis—converting glucose to lactate despite oxygen availability—thereby enabling rapid ATP production and the diversion of glycolytic intermediates into biosynthetic pathways [6, 7]. In the current study, among the twelve cancers harmonized by Hu et al.

(2025), the CellFie tasks, ATP generation from glucose (hypoxic conditions) – glycolysis, and glucose to lactate conversion are both upregulated in ESCC, KIRC, LUAD, LUSC, and OV (Fig. S5), while the normal tissues of other cancer types exhibited high baseline aerobic glycolysis activities (Fig. S7). Concomitantly, auxiliary pathways such as the pentose phosphate pathway (PPP) are activated to maintain redox homeostasis through NADPH production and to facilitate nucleotide biosynthesis [2, 3, 5]. Correspondingly, the PPP-related CellFie task, ribose-5-phosphate synthesis was upregulated in COAD, GBM, KIRC, LIHC, and UCEC in the Hu2025-harmonized datasets (Fig. S5), while other cancer types demonstrated robust baseline activity of ribose-5-phosphate synthesis (Fig. S7). Despite the prominent reliance on glycolysis, many cancers retain an active tricarboxylic acid (TCA) cycle and oxidative phosphorylation (OXPHOS), often fueled by alternative substrates such as glutamine and fatty acids [1, 8, 9]. Our data indicate that the CellFie task, krebs cycle – NADH generation is upregulated in COAD, ESCC, LIHC, LUAD, and LUSC, but downregulated in GBM, HNSC, STAD, and PAAD, inversely correlating with their baseline activities in matched normal tissues (Figs. S5 & S7). This metabolic plasticity enables cancer cells to flexibly generate energy and biosynthetic precursors under diverse microenvironmental conditions.

Moreover, lactate accumulation—a byproduct of aerobic glycolysis—acidifies the tumor microenvironment, thereby promoting immune evasion, angiogenesis, and metastasis [5].

Altered vitamine & cofactor metabolism in cancer: implications for ROS stress and epigenetic regulation

Altered vitamin and cofactor metabolism plays a critical role in modulating ROS stress and shaping the epigenetic landscape in cancer. Vitamins from the B-complex group act as precursors for essential coenzymes—including NAD□, flavin adenine dinucleotide (FAD□),

and coenzyme A (e.g., acetyl-CoA)—which are integral to cellular metabolism (such as TCA cycle) and maintenance of redox balance [1, 2]. Moreover, dysregulation of these metabolic pathways can influence epigenetic modifications; for example, acetyl-CoA serves as a substrate for histone acetylation, thereby affecting chromatin structure and gene expression [52]. Additionally, B vitamins such as B6, B9, and B12 support pathways that maintain S-adenosylmethionine (SAM) levels and its methylation capacity, with SAM functioning as a methyl donor for DNA methylation [53]. In the current study, synthesis of coenzyme NAD was significantly upregulated in eight out of the twelve cancer types harmonized by Hu et al. (2025) (Figs. 4B and S5), likely compensating for their relatively low baseline activity observed in matched normal tissues (Fig. S7). Baseline activities of coenzyme A biosynthesis were relatively higher (than synthesis of coenzyme NAD) in normal tissues, with compensatory upregulation noted in the four cancer types exhibiting lower baseline levels (Figs. S5 and S7). Furthermore, the SAM-related metabolic task, S-adenosyl-L-methionine synthesis, was upregulated in five cancer types (ESCC, KIRC, LUAD, LUSC, and OV) of the Hu2025-harmonized datasets, again compensating for lower baseline activities in corresponding normal tissues (Figs. S5 and S7). Collectively, these interconnected metabolic alterations may enable cancer cells to fine-tune their epigenetic regulation and redox state, thereby promoting proliferation, therapeutic resistance, and metastatic potential.

Conclusion

Collectively, our findings present a comprehensive atlas of metabolic remodeling across diverse cancer types, highlighting both conserved and context-specific aspects of tumor metabolism. By utilizing publicly available pan-cancer proteomics datasets, we quantified metabolic activities at the task level, thereby complementing existing metabolite-centric analyses and unveiling new opportunities for precision targeting of metabolic vulnerabilities.

Future studies should explore how these metabolic signatures correlate with specific driver mutations, tumor progression stages, involved cell types, and the tumor microenvironment, ultimately informing the development of metabolism-based therapeutic strategies.

List of abbreviations

ATP	Adenosine triphosphate
TCA	Tricarboxylic acid
NADPH	Nicotinamide adenine dinucleotide phosphate
PPP	Pentose phosphate pathway
ME1/2	Malic enzyme
IDH1/2	Cytosolic/mitochondrial isocitrate dehydrogenases
ROS	Reactive oxygen species
HIFs	Hypoxia-inducible factors
acetyl-CoA	Acetyl coenzyme A
SAM	S-adenosylmethionine
DNA	Deoxyribonucleic acid
BRCA	Breast invasive ductal carcinoma
COAD	Colon adenocarcinoma
ESCC	Esophageal squamous cell carcinoma
GBM	Glioblastoma
HNSC	Head and neck squamous cell carcinoma
KIRC	Kidney renal clear cell carcinoma
LIHC	Liver hepatocellular carcinoma
LUAD	Lung adenocarcinoma
LUSC	Lung squamous cell carcinoma

OV	Ovarian serous cystadenocarcinoma
PAAD	Pancreatic adenocarcinoma
STAD	Stomach adenocarcinoma
UCEC	Uterine corpus endometrial carcinoma
BLCA	Bladder invasive urothelial carcinoma
PRAD	Prostate adenocarcinoma
SCLC	Lung small cell carcinoma
MS	Mass sepctrometry
FDR	False discovery rate
CPTAC	Clinical Proteomic Tumor Analysis Consortium
PRIDE	Proteomics IDentifications Exchange
logFC	Log fold change
p.adj	Adjusted p-value
RNA	Ribonucleic acid
FAD	Flavin adenine dinucleotide (oxidized form)
SAM	S-adenosylmethionine

Authors' contributions

Y.L. conceived and designed the study; Y.L., Y.B. and Q.C. analyzed the data, prepared figures and/or tables. Y.L., Y.B. and Q.C. wrote the paper. All authors read and approved the final manuscript.

Availability of data and materials

All data generated during this study are included in this published article [and its additional files]

Funding

This work is supported by the Chinese Government Scholarship (Grant no. 202108515040), Sichuan Healthcare Commission Science and Technology Project (Grant no. 24QNMP006), Nanchong City-School Science and Technology Cooperation Special Project (Grant no. 22SXQT0096) and 2023 North Sichuan Medical College Research and Development Fund Project (CBY23-ZDA11). The funders had no role in study design, data analysis, decision to publish, or preparation of the manuscript.

Declaration of interests

On behalf of all authors, the corresponding author states that there is no conflict of interest.

References

1. DeBerardinis RJ, Chandel NS. Fundamentals of cancer metabolism. Sci Adv. 2016;2(5):e1600200.
2. Pavlova NN, Zhu J, Thompson CB. The hallmarks of cancer metabolism: Still emerging. Cell Metab. 2022;34(3):355-77.
3. Martínez-Reyes I, Chandel NS. Cancer metabolism: looking forward. Nat Rev Cancer. 2021;21(10):669-80.
4. Yang J, Shay C, Saba NF, Teng Y. Cancer metabolism and carcinogenesis. Exp hematol oncol. 2024;13(1):10.
5. Boroughs LK, DeBerardinis RJ. Metabolic pathways promoting cancer cell survival and growth. Nat Cell Biol. 2015;17(4):351-9.
6. Lunt SY, Vander Heiden MG. Aerobic glycolysis: meeting the metabolic requirements of cell proliferation. Annu Rev Cell Dev Biol. 2011;27(1):441-64.
7. Koppenol WH, Bounds PL, Dang CV. Otto Warburg's contributions to current concepts of cancer metabolism. Nat Rev Cancer. 2011;11(5):325-37.

8. Corbet C, Pinto A, Martherus R, de Jesus JP, Polet F, Feron O. Acidosis drives the reprogramming of fatty acid metabolism in cancer cells through changes in mitochondrial and histone acetylation. Cell Metab. 2016;24(2):311-23.
9. Nan D, Yao W, Huang L, Liu R, Chen X, Xia W, Sheng H, Zhang H, Liang X, Lu Y. Glutamine and cancer: Metabolism, immune microenvironment, and therapeutic targets. Cell Commun Signal. 2025;23(1):45.
10. Pang B, Wu H. Metabolic reprogramming in colorectal cancer: a review of aerobic glycolysis and its therapeutic implications for targeted treatment strategies. Cell Death Discov. 2025;11(1):321.
11. Xu M, Zhang T, Xia R, Wei Y, Wei X. Targeting the tumor stroma for cancer therapy. Mol cancer. 2022;21(1):208.
12. Zhang J, Yao M, Xia S, Zeng F, Liu Q. Systematic and comprehensive insights into HIF-1 stabilization under normoxic conditions: implications for cellular adaptation and therapeutic strategies in cancer. Cell Mol Biol Lett. 2025;30(1):2.
13. Lynch TP, Ferrer CM, Jackson SR, Shahriari KS, Vosseller K, Reginato MJ. Critical role of O-Linked β-N-acetylglucosamine transferase in prostate cancer invasion, angiogenesis, and metastasis. J Biol Chem. 2012;287(14):11070-81.
14. Pienkowski T, Wawrzak-Pienkowska K, Tankiewicz-Kwedlo A, Ciborowski M, Kurek K, Pawlak D. Leveraging glycosylation for early detection and therapeutic target discovery in pancreatic cancer. Cell Death Dis. 2025;16(1):227.
15. Lyssiotis CA, Kimmelman AC. Metabolic interactions in the tumor microenvironment. Trends Cell Biol. 2017;27(11):863-75.
16. Giuliani S, Accetta C, di Martino S, De Vitis C, Messina E, Pescarmona E, Fanciulli M, Ciliberto G, Mancini R, Falcone I. Metabolic Reprogramming in Melanoma: An Epigenetic Point of View. Pharmaceuticals. 2025;18(6):853.

17. Zhang Y, Song H, Li M, Lu P. Histone lactylation bridges metabolic reprogramming and epigenetic rewiring in driving carcinogenesis: Oncometabolite fuels oncogenic transcription. Clin Transl Med. 2024;14(3):e1614.
18. Capatina AL, Malcolm JR, Stenning J, Moore RL, Bridge KS, Brackenbury WJ, Holding AN. Hypoxia-induced epigenetic regulation of breast cancer progression and the tumour microenvironment. Front cell dev biol. 2024;12:1421629.
19. Yin L, Zhang J, Zhu Z, Peng X, Lan H, Ayoub A, Tan M, Zhou B, He Y, Wang S, Lu Y. The FBXW7–KMT2 axis in cancer-associated fibroblasts controls tumor growth via an epigenetic-paracrine mechanism. PNAS. 2025;122(13):e2423130122.
20. Mullen NJ, Singh PK. Nucleotide metabolism: a pan-cancer metabolic dependency. Nat Rev Cancer. 2023;23(5):275-94.
21. Rosario SR, Long MD, Affronti HC, Rowsam AM, Eng KH, Smiraglia DJ. Pan-cancer analysis of transcriptional metabolic dysregulation using The Cancer Genome Atlas. Nat Comm. 2018;9(1):5330.
22. Schneider G, Schmidt-Supprian M, Rad R, Saur D. Tissue-specific tumorigenesis: context matters. Nat Rev Cancer. 2017;17(4):239-53.
23. Richelle A, Kellman BP, Wenzel AT, Chiang AW, Reagan T, Gutierrez JM, Joshi C, Li S, Liu JK, Masson H, Lee J. Model-based assessment of mammalian cell metabolic functionalities using omics data. Cell Rep Methods. 2021;1(3).
24. Zhou Y, Lih TM, Pan J, Höti N, Dong M, Cao L, Hu Y, Cho KC, Chen SY, Eguez RV, Gabrielson E. Proteomic signatures of 16 major types of human cancer reveal universal and cancer-type-specific proteins for the identification of potential therapeutic targets. J Hematol Oncol. 2020;13(1):170.

25. Vasaikar S, Huang C, Wang X, Petyuk VA, Savage SR, Wen B, Dou Y, Zhang Y, Shi Z, Arshad OA, Gritsenko MA. Proteogenomic analysis of human colon cancer reveals new therapeutic opportunities. Cell. 2019;177(4):1035-49.
26. Liu W, Xie L, He YH, Wu ZY, Liu LX, Bai XF, Deng DX, Xu XE, Liao LD, Lin W, Heng JH. Large-scale and high-resolution mass spectrometry-based proteomics profiling defines molecular subtypes of esophageal cancer for therapeutic targeting. Nat Commun. 2021;12(1):4961.
27. Wang LB, Karpova A, Gritsenko MA, Kyle JE, Cao S, Li Y, Rykunov D, Colaprico A, Rothstein JH, Hong R, Stathias V. Proteogenomic and metabolomic characterization of human glioblastoma. Cancer cell. 2021;39(4):509-28.
28. Huang C, Chen L, Savage SR, Eguez RV, Dou Y, Li Y, da Veiga Leprevost F, Jaehnig EJ, Lei JT, Wen B, Schnaubelt M. Proteogenomic insights into the biology and treatment of HPV-negative head and neck squamous cell carcinoma. Cancer cell. 2021;39(3):361-79.
29. Clark DJ, Dhanasekaran SM, Petralia F, Pan J, Song X, Hu Y, da Veiga Leprevost F, Reva B, Lih TS, Chang HY, Ma W. Integrated proteogenomic characterization of clear cell renal cell carcinoma. Cell. 2019;179(4):964-83.
30. Gao Q, Zhu H, Dong L, Shi W, Chen R, Song Z, Huang C, Li J, Dong X, Zhou Y, Liu Q. Integrated proteogenomic characterization of HBV-related hepatocellular carcinoma. Cell. 2019;179(2):561-77.
31. Gillette MA, Satpathy S, Cao S, Dhanasekaran SM, Vasaikar SV, Krug K, Petralia F, Li Y, Liang WW, Reva B, Krek A. Proteogenomic characterization reveals therapeutic vulnerabilities in lung adenocarcinoma. Cell. 2020;182(1):200-25.

32. Satpathy S, Krug K, Beltran PM, Savage SR, Petralia F, Kumar-Sinha C, Dou Y, Reva B, Kane MH, Avanessian SC, Vasaikar SV. A proteogenomic portrait of lung squamous cell carcinoma. Cell. 2021;184(16):4348-71.
33. McDermott JE, Arshad OA, Petyuk VA, Fu Y, Gritsenko MA, Clauss TR, Moore RJ, Schepmoes AA, Zhao R, Monroe ME, Schnaubelt M. Clinical Proteomic Tumor Analysis Consortium Proteogenomic characterization of ovarian HGSC implicates mitotic kinases, replication stress in observed chromosomal instability. Cell Rep Med. 2020;1:100004.
34. Cao L, Huang C, Zhou DC, Hu Y, Lih TM, Savage SR, Krug K, Clark DJ, Schnaubelt M, Chen L, da Veiga Leprevost F. Proteogenomic characterization of pancreatic ductal adenocarcinoma. Cell. 2021;184(19):5031-52.
35. Mun DG, Bhin J, Kim S, Kim H, Jung JH, Jung Y, Jang YE, Park JM, Kim H, Jung Y, Lee H. Proteogenomic characterization of human early-onset gastric cancer. Cancer cell. 2019;35(1):111-24.
36. Dou Y, Kawaler EA, Zhou DC, Gritsenko MA, Huang C, Blumenberg L, Karpova A, Petyuk VA, Savage SR, Satpathy S, Liu W. Proteogenomic characterization of endometrial carcinoma. Cell. 2020;180(4):729-48.
37. Hu GS, Zheng ZZ, He YH, Wang DC, Nie RC, Liu W. Integrated Analysis of Proteome and Transcriptome Profiling Reveals Pan-Cancer-Associated Pathways and Molecular Biomarkers. Mol Cell Proteomics. 2025;24(3).
38. Edwards NJ, Oberti M, Thangudu RR, Cai S, McGarvey PB, Jacob S, Madhavan S, Ketchum KA. The CPTAC data portal: a resource for cancer proteomics research. J Proteome Res. 2015;14(6):2707-13.

39. Ritchie ME, Phipson B, Wu DI, Hu Y, Law CW, Shi W, Smyth GK. limma powers differential expression analyses for RNA-sequencing and microarray studies. Nucleic Acids Res. 2015;43(7):e47-.
40. Mayers JR, Torrence ME, Danai LV, Papagiannakopoulos T, Davidson SM, Bauer MR, Lau AN, Ji BW, Dixit PD, Hosios AM, Muir A. Tissue of origin dictates branched-chain amino acid metabolism in mutant Kras-driven cancers. Science. 2016;353(6304):1161-5.
41. Yuneva MO, Fan TW, Allen TD, Higashi RM, Ferraris DV, Tsukamoto T, Matés JM, Alonso FJ, Wang C, Seo Y, Chen X. The metabolic profile of tumors depends on both the responsible genetic lesion and tissue type. Cell Metab. 2012;15(2):157-70.
42. Pinho SS, Reis CA. Glycosylation in cancer: mechanisms and clinical implications. Nat Rev Cancer. 2015;15(9):540-55.
43. Wang H, Mooney DJ. Metabolic glycan labelling for cancer-targeted therapy. Nat Chem. 2020;12(12):1102-14.
44. Vajaria BN, Patel PS. Glycosylation: a hallmark of cancer?. Glycoconj J. 2017;34(2):147-56.
45. Shi DD, Savani MR, Abdullah KG, McBrayer SK. Emerging roles of nucleotide metabolism in cancer. Trends Cancer. 2023;9(8):624-35.
46. Chen J, Cui L, Lu S, Xu S. Amino acid metabolism in tumor biology and therapy. Cell Death Dis. 2024;15(1):42.
47. Lieu EL, Nguyen T, Rhyne S, Kim J. Amino acids in cancer. Exp Mol Med. 2020;52(1):15-30.
48. Medina MA. Glutamine and cancer. J Nutr. 2001;131(9):2539S-42S.
49. Lukey MJ, Katt WP, Cerione RA. Targeting amino acid metabolism for cancer therapy. Drug Discov Today. 2017;22(5):796-804.

50. Patel D, Menon D, Bernfeld E, Mroz V, Kalan S, Loayza D, Foster DA. Aspartate rescues S-phase arrest caused by suppression of glutamine utilization in KRas-driven cancer cells. J biol chem. 2016;291(17):9322-9.
51. Casero Jr RA, Murray Stewart T, Pegg AE. Polyamine metabolism and cancer: treatments, challenges and opportunities. Nat Rev Cancer. 2018;18(11):681-95.
52. Bradshaw PC. Acetyl-CoA metabolism and histone acetylation in the regulation of aging and lifespan. Antioxidants. 2021;10(4):572.
53. Fernández-Ramos D, Lopitz-Otsoa F, Lu SC, Mato JM. S-adenosylmethionine: a multifaceted regulator in cancer pathogenesis and therapy. Cancers. 2025;17(3):535.

Figure legeneds

Figure 1. Sample and Metabolic Task Summaries. This figure presents the sample sizes for the Zhou2020 (A) and Hu2025-harmonized (B) datasets, alongside the identified metabolic tasks in the Zhou2020 (C) and Hu2025-harmonized (D) datasets.

Figure 2. Metabolic rewiring as an inverse response to normal metabolic activities in the Zhou2020 dataset. This figure illustrates the total percentage of active metabolic tasks across all tasks, as well as within each of the seven metabolic systems, for different cancer types in both normal (A) and tumor tissues (B). C) presents bar plots depicting the number of differentially upregulated and downregulated tasks, subsystems, and systems across 15 cancer types, with red indicating upregulation and blue indicating downregulation. D) Dotplot of Pearson correlations between the baseline percentage of active tasks in normal tissues and the log fold change of task scores comparing tumor to normal tissues. Correlation coefficients were calculated separately for each cancer type, based on a sample size of 176.

Figure 3. Metabolic rewiring as an inverse response to normal metabolic activities in the Hu2025-harmonized datasets. This figure illustrates the total percentage of active metabolic tasks across all tasks, as well as within each of the seven metabolic systems, for different cancer types in both normal (A) and tumor tissues (B). C) presents bar plots depicting the number of differentially upregulated and downregulated tasks, subsystems, and systems across twelve cancer types, with red indicating upregulation and blue indicating downregulation. D) Dotplot of Pearson correlations between the baseline percentage of active tasks in normal tissues and the log fold change of task scores comparing tumor to normal tissues. Correlation coefficients were calculated separately for each cancer type, based on a sample size of 138.

Figure 4. Significantly dysregulated metabolic tasks (B), subsystems (A), and systems (C) in the Hu2025-harmonized datasets. For the dysregulated tasks, only the top ones—those up- or downregulated in eight or more cancer types—are shown, while the full list is available in Figure S5.

Figure 5. Significantly disregulated metabolic tasks (B), subsystems (A) and systems (C) in the Zhou2020 dataset. For the disregulated tasks, only the top ones—those up- or downregulated in fiveor more cancer types—are shown, while the full list can be found in Figure S6.

Additional files

FigureS1.pdf: Figure S1. Upset plots illustrating both shared and unique dysregulated tasks across different cancer types and studies. A) Upregulated tasks. B) Downregulated tasks.

FigureS2.pdf: Figure S2. Upset plots illustrating both shared and unique dysregulated subsystems across different cancer types and studies. A) Upregulated subsystems. B) Downregulated subsystems.

FigureS3.pdf: Figure S3. Upset plots illustrating both shared and unique dysregulated systems across different cancer types and studies. A) Upregulated systems. B) Downregulated systems.

FigureS4.pdf: Figure S4. Volcano plots displaying upregulated and downregulated tasks, subsystems, and systems across different cancer types and datasets. A) shows the twelve cancer types in the Hu2025-harmonized datasets. B) presents 15 cancer types from the Zhou2020 dataset. Red dots represent upregulated tasks, subsystems, or systems, and blue dots indicate downregulated ones. The smallest dots correspond to metabolic tasks, medium-sized dots represent subsystems, and the largest dots denote systems. The top tasks, subsystems, and systems are also labeled.

FigureS5.pdf: Figure S5. Significantly disregulated metabolic tasks in the Hu2025-harmonized datasets.

FigureS6.pdf: Figure S6. Significantly disregulated metabolic tasks in the Zhou2020 dataset.

FigureS7.pdf: Figure S7. Task-level baseline metabolic activities in normal tissues from the Hu2025-harmonized datasets. Both the size and color of the dots represent the percentage of active tasks across normal samples.

FigureS8.pdf: Figure S8. Task-level baseline metabolic activities in normal tissues from the Zhou2020 dataset. Both the size and color of the dots represent the percentage of active tasks across normal samples.

FigureS9.pdf: Figure S9. Subsystem-level baseline metabolic activities in normal tissues from the Hu2025-harmonized datasets. Both the size and color of the dots represent the percentage of active tasks across normal samples.

FigureS10.pdf: Figure S10. Subsystem-level baseline metabolic activities in normal tissues from the Zhou2020 dataset. Both the size and color of the dots represent the percentage of active tasks across normal samples.

TableS1.xlsx: Table S1. Dataset information.

TableS2.xlsx: Table S2. Sample information.

TableS3.xlsx: Table S3. Metabolic activity scores at different depths for different datasets.

TableS4.xlsx: Table S4. Percentages of active metabolic tasks.

TableS5.xlsx: Table S5. Limma differentiall analysis result tables.

TableS6.xlsx: Table S6. Inverse correlation between normal active task percentage and caner metabolic rewiring (logFC of task scores).

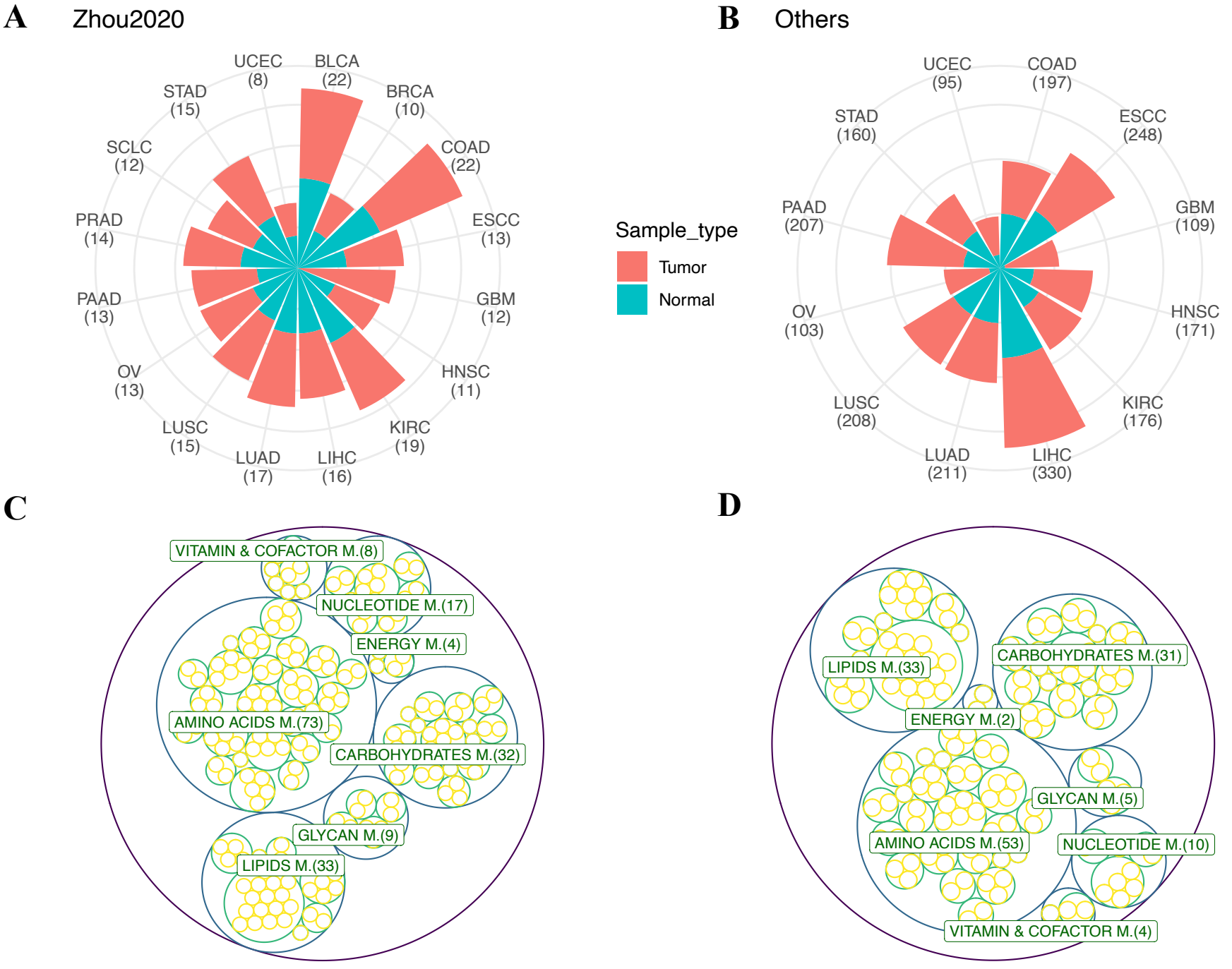
A
Zhou2020
UCEC (8)
BLCA (22)
BRCA (10)
COAD (22)
ESCC (13)
GBM (12)
HNSC (11)
KIRC (19)
LIHC (16)
LUAD (17)
LUSC (15)
OV (13)
PAAD (13)
PRAD (14)
SCLC (12)
STAD (15)
Sample_type
Tumor
Normal
B
Others
UCEC (95)
COAD (197)
ESCC (248)
GBM (109)
HNSC (171)
KIRC (176)
LIHC (330)
LUAD (211)
LUSC (208)
OV (103)
PAAD (207)
STAD (160)
C
VITAMIN & COFACTOR M.(8)
NUCLEOTIDE M.(17)
ENERGY M.(4)
AMINO ACIDS M.(73)
CARBOHYDRATES M.(32)
GLYCAN M.(9)
LIPIDS M.(33)
D
LIPIDS M.(33)
CARBOHYDRATES M.(31)
ENERGY M.(2)
GLYCAN M.(5)
AMINO ACIDS M.(53)
NUCLEOTIDE M.(10)
VITAMIN & COFACTOR M.(4)

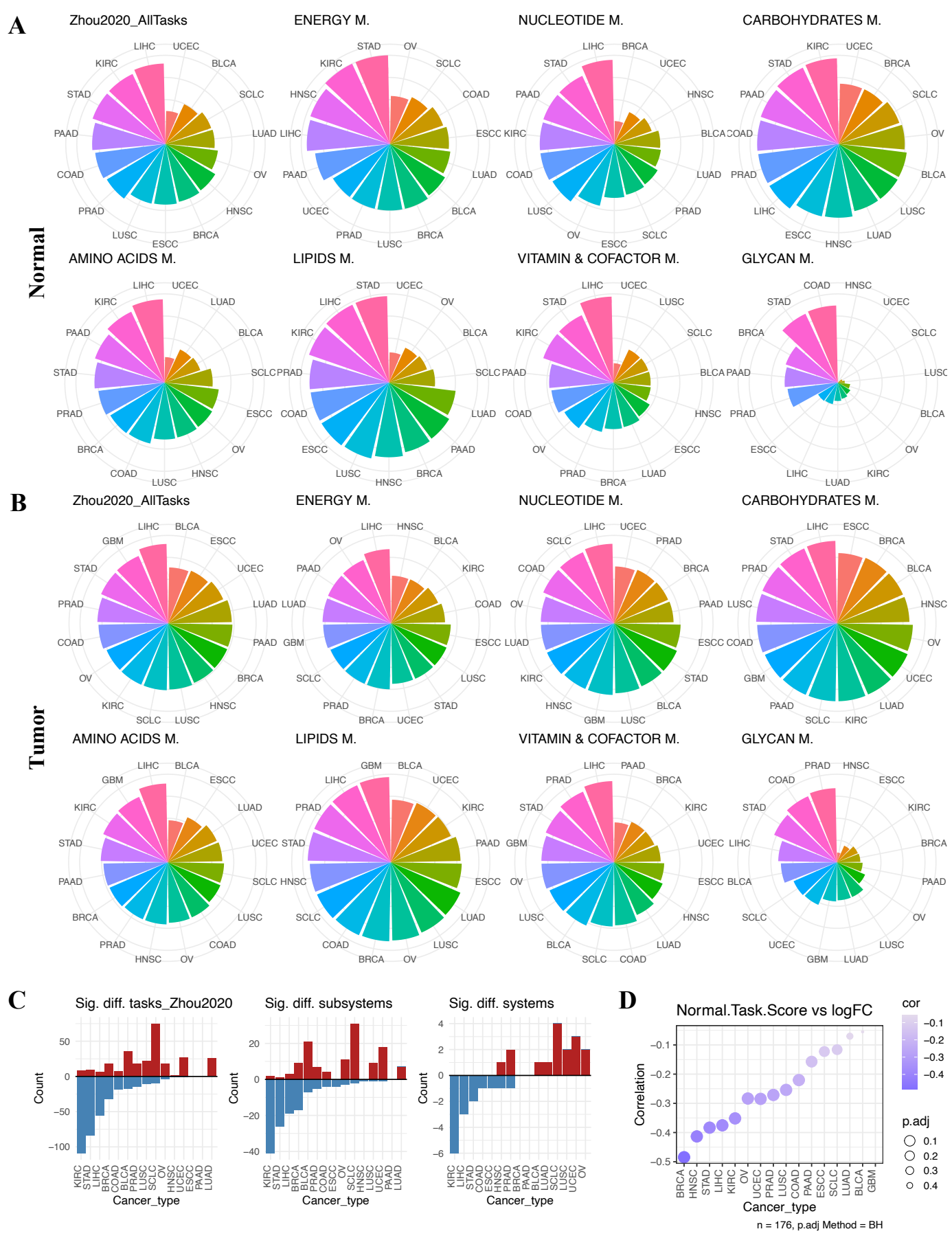
A
Normal
Zhou2020_AllTasks
ENERGY M.
NUCLEOTIDE M.
CARBOHYDRATES M.
AMINO ACIDS M.
LIPIDS M.
VITAMIN & COFACTOR M.
GLYCAN M.
B
Tumor
Zhou2020_AllTasks
ENERGY M.
NUCLEOTIDE M.
CARBOHYDRATES M.
AMINO ACIDS M.
LIPIDS M.
VITAMIN & COFACTOR M.
GLYCAN M.
C
Sig. diff. tasks_Zhou2020
Sig. diff. subsystems
Sig. diff. systems
Count
Cancer_type
D
Normal.Task.Score vs logFC
Correlation
Cancer_type
cor
p.adj
n = 176, p.adj Method = BH

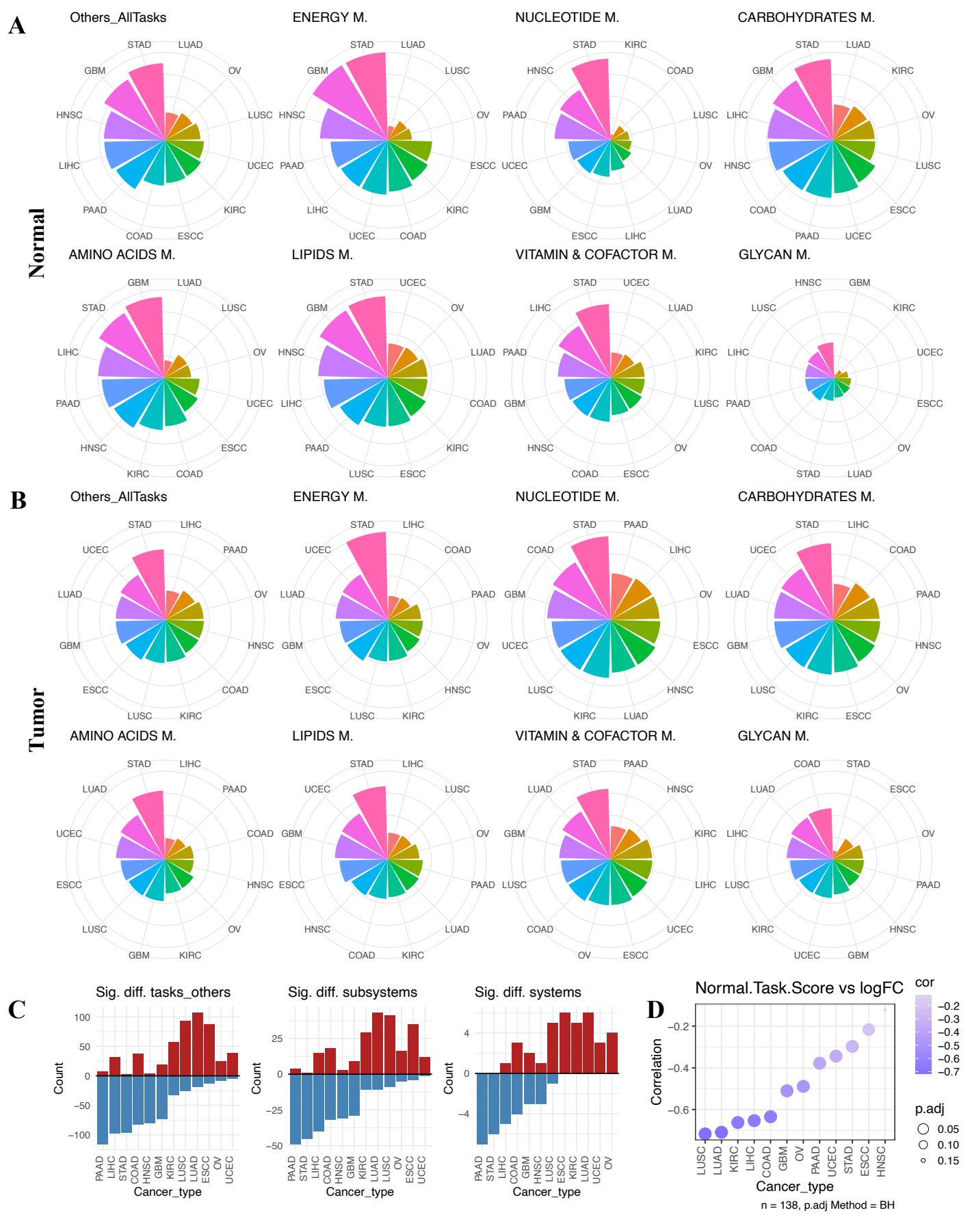
A
Normal
Others_AllTasks
ENERGY M.
NUCLEOTIDE M.
CARBOHYDRATES M.
AMINO ACIDS M.
LIPIDS M.
VITAMIN & COFACTOR M.
GLYCAN M.
B
Tumor
Others_AllTasks
ENERGY M.
NUCLEOTIDE M.
CARBOHYDRATES M.
AMINO ACIDS M.
LIPIDS M.
VITAMIN & COFACTOR M.
GLYCAN M.
C
Sig. diff. tasks_others
Sig. diff. subsystems
Sig. diff. systems
Count
Cancer_type
D
Normal.Task.Score vs logFC
Correlation
Cancer_type
cor
p.adj
0.05
0.10
0.15
n = 138, p.adj Method = BH

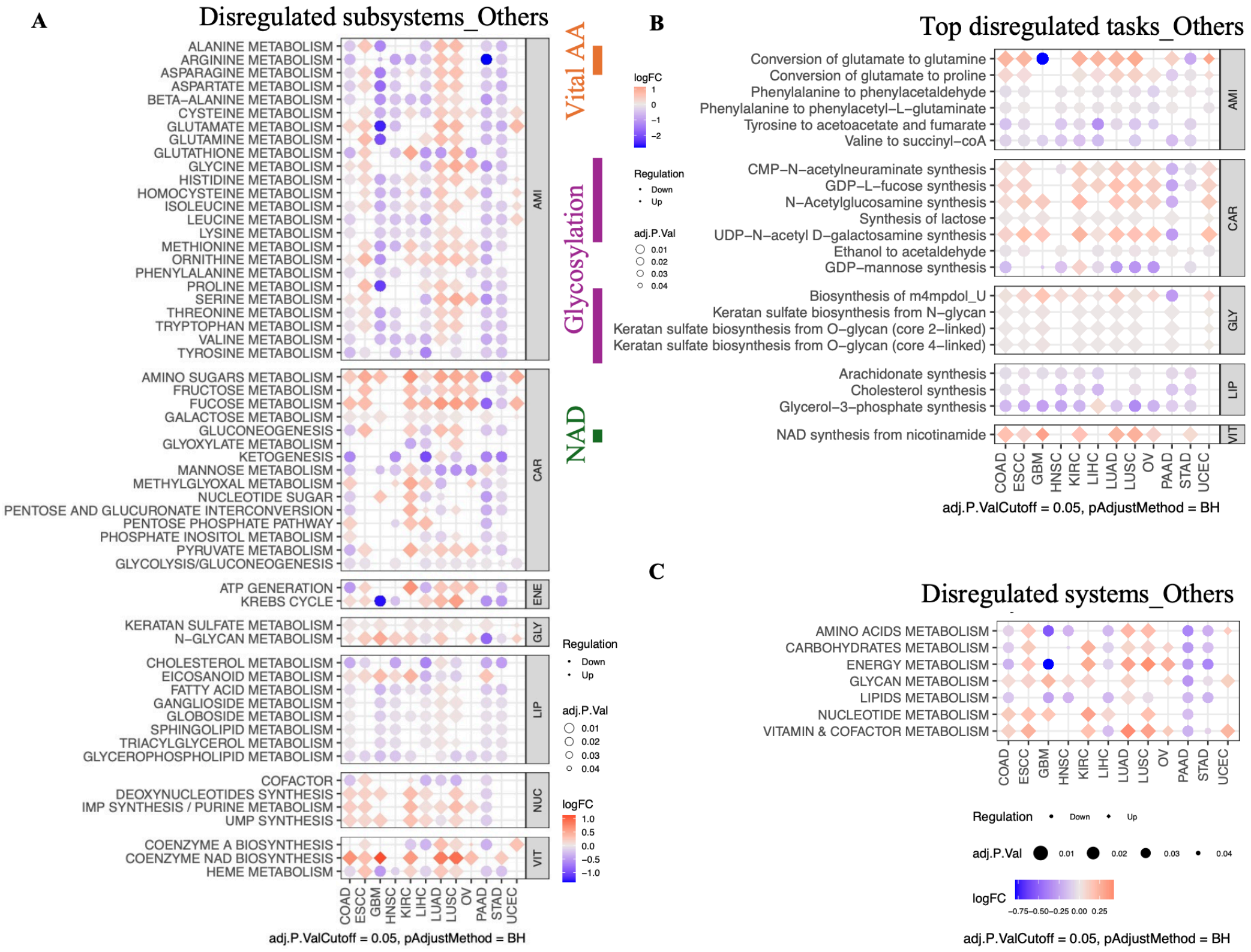
A
Disregulated subsystems_Others
ALANINE METABOLISM
ARGININE METABOLISM
ASPARAGINE METABOLISM
ASPARTATE METABOLISM
BETA–ALANINE METABOLISM
CYSTEINE METABOLISM
GLUTAMATE METABOLISM
GLUTAMINE METABOLISM
GLUTATHIONE METABOLISM
GLYCINE METABOLISM
HISTIDINE METABOLISM
HOMOCYSTEINE METABOLISM
ISOLEUCINE METABOLISM
LEUCINE METABOLISM
LYSINE METABOLISM
METHIONINE METABOLISM
ORNITHINE METABOLISM
PHENYLALANINE METABOLISM
PROLINE METABOLISM
SERINE METABOLISM
THREONINE METABOLISM
TRYPTOPHAN METABOLISM
VALINE METABOLISM
TYROSINE METABOLISM
AMI
AMINO SUGARS METABOLISM
FRUCTOSE METABOLISM
FUCOSE METABOLISM
GALACTOSE METABOLISM
GLUCONEOGENESIS
GLYOXYLATE METABOLISM
KETOGENESIS
MANNOSE METABOLISM
METHYLGLYOXAL METABOLISM
NUCLEOTIDE SUGAR
PENTOSE AND GLUCURONATE INTERCONVERSION
PENTOSE PHOSPHATE PATHWAY
PHOSPHATE INOSITOL METABOLISM
PYRUVATE METABOLISM
GLYCOLYSIS/GLUCONEOGENESIS
CAR
ATP GENERATION
KREBS CYCLE
ENE
KERATAN SULFATE METABOLISM
N–GLYCAN METABOLISM
GLY
CHOLESTEROL METABOLISM
EICOSANOID METABOLISM
FATTY ACID METABOLISM
GANGLIOSIDE METABOLISM
GLOBOSIDE METABOLISM
SPHINGOLIPID METABOLISM
TRIACYLGLYCEROL METABOLISM
GLYCEROPHOSPHOLIPID METABOLISM
LIP
COFACTOR
DEOXYNUCLEOTIDES SYNTHESIS
IMP SYNTHESIS / PURINE METABOLISM
UMP SYNTHESIS
NUC
COENZYME A BIOSYNTHESIS
COENZYME NAD BIOSYNTHESIS
HEME METABOLISM
VIT
COAD ESCC GBM HNSC KIRC LIHC LUAD LUSC OV PAAD STAD UCEC
adj.P.ValCutoff = 0.05, pAdjustMethod = BH
Vital AA
Glycosylation
NAD
logFC
1
0
−1
−2
Regulation
Down
Up
adj.P.Val
0.01
0.02
0.03
0.04
B
Top disregulated tasks_Others
Conversion of glutamate to glutamine
Conversion of glutamate to proline
Phenylalanine to phenylacetaldehyde
Phenylalanine to phenylacetyl–L–glutaminate
Tyrosine to acetoacetate and fumarate
Valine to succinyl–coA
AMI
CMP–N–acetylneuraminate synthesis
GDP–L–fucose synthesis
N–Acetylglucosamine synthesis
Synthesis of lactose
UDP–N–acetyl D–galactosamine synthesis
Ethanol to acetaldehyde
GDP–mannose synthesis
CAR
Biosynthesis of m4mpdol_U
Keratan sulfate biosynthesis from N–glycan
Keratan sulfate biosynthesis from O–glycan (core 2–linked)
Keratan sulfate biosynthesis from O–glycan (core 4–linked)
GLY
Arachidonate synthesis
Cholesterol synthesis
Glycerol–3–phosphate synthesis
LIP
NAD synthesis from nicotinamide
VIT
COAD ESCC GBM HNSC KIRC LIHC LUAD LUSC OV PAAD STAD UCEC
adj.P.ValCutoff = 0.05, pAdjustMethod = BH
C
Disregulated systems_Others
AMINO ACIDS METABOLISM
CARBOHYDRATES METABOLISM
ENERGY METABOLISM
GLYCAN METABOLISM
LIPIDS METABOLISM
NUCLEOTIDE METABOLISM
VITAMIN & COFACTOR METABOLISM
COAD ESCC GBM HNSC KIRC LIHC LUAD LUSC OV PAAD STAD UCEC
Regulation Down Up
adj.P.Val 0.01 0.02 0.03 0.04
logFC
−0.75 −0.50 −0.25 0.00 0.25
adj.P.ValCutoff = 0.05, pAdjustMethod = BH

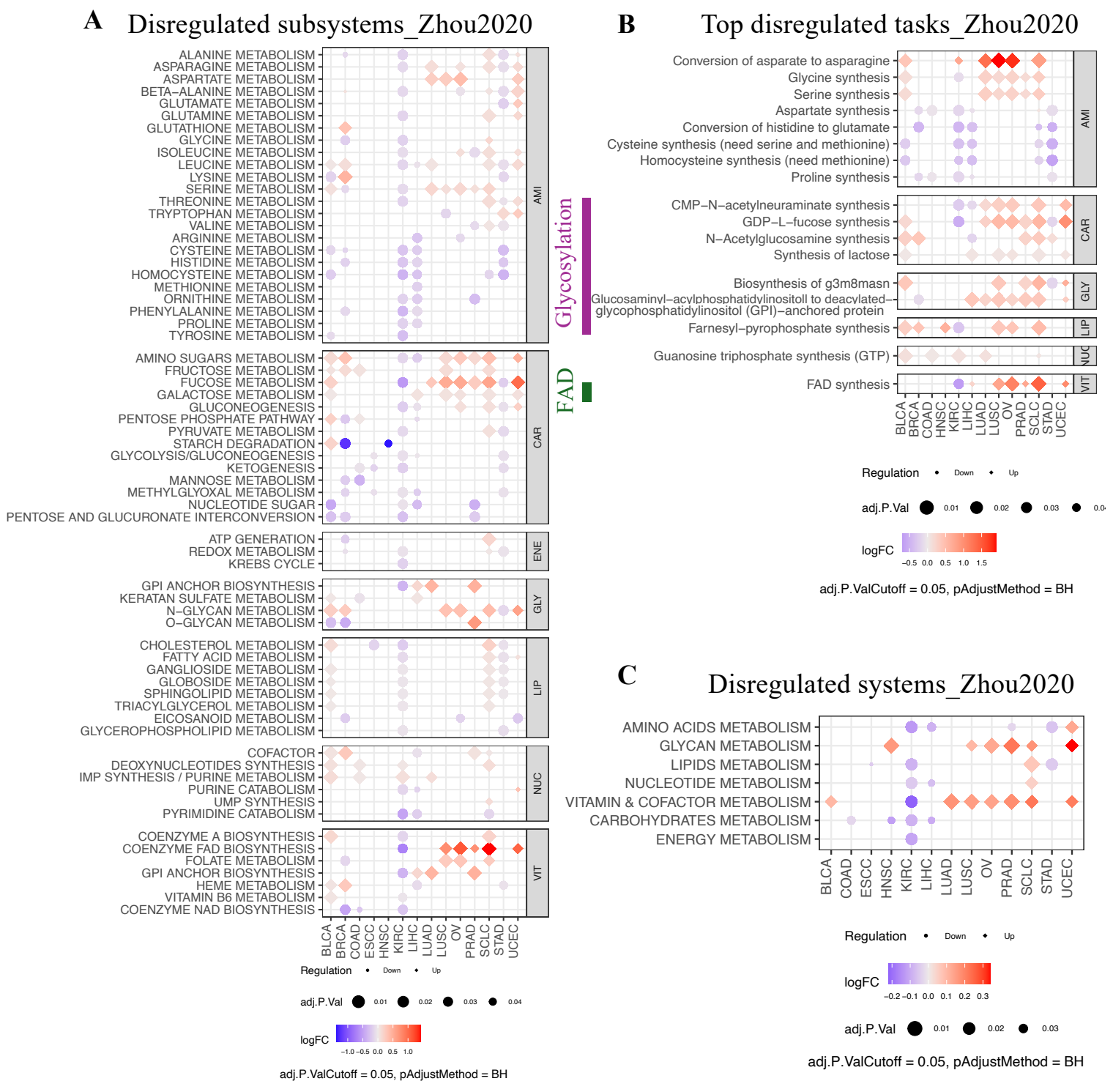
A
Disregulated subsystems_Zhou2020
ALANINE METABOLISM
ASPARAGINE METABOLISM
ASPARTATE METABOLISM
BETA−ALANINE METABOLISM
GLUTAMATE METABOLISM
GLUTAMINE METABOLISM
GLUTATHIONE METABOLISM
GLYCINE METABOLISM
ISOLEUCINE METABOLISM
LEUCINE METABOLISM
LYSINE METABOLISM
SERINE METABOLISM
THREONINE METABOLISM
TRYPTOPHAN METABOLISM
VALINE METABOLISM
ARGININE METABOLISM
CYSTEINE METABOLISM
HISTIDINE METABOLISM
HOMOCYSTEINE METABOLISM
METHIONINE METABOLISM
ORNITHINE METABOLISM
PHENYLALANINE METABOLISM
PROLINE METABOLISM
TYROSINE METABOLISM
AMI
AMINO SUGARS METABOLISM
FRUCTOSE METABOLISM
FUCOSE METABOLISM
GALACTOSE METABOLISM
GLUCONEOGENESIS
PENTOSE PHOSPHATE PATHWAY
PYRUVATE METABOLISM
STARCH DEGRADATION
GLYCOLYSIS/GLUCONEOGENESIS
KETOGENESIS
MANNOSE METABOLISM
METHYLGLYOXAL METABOLISM
NUCLEOTIDE SUGAR
PENTOSE AND GLUCURONATE INTERCONVERSION
CAR
ATP GENERATION
REDOX METABOLISM
KREBS CYCLE
ENE
GPI ANCHOR BIOSYNTHESIS
KERATAN SULFATE METABOLISM
N−GLYCAN METABOLISM
O−GLYCAN METABOLISM
GLY
CHOLESTEROL METABOLISM
FATTY ACID METABOLISM
GANGLIOSIDE METABOLISM
GLOBOSIDE METABOLISM
SPHINGOLIPID METABOLISM
TRIACYLGLYCEROL METABOLISM
EICOSANOID METABOLISM
GLYCEROPHOSPHOLIPID METABOLISM
LIP
COFACTOR
DEOXYNUCLEOTIDES SYNTHESIS
IMP SYNTHESIS / PURINE METABOLISM
PURINE CATABOLISM
UMP SYNTHESIS
PYRIMIDINE CATABOLISM
NUC
COENZYME A BIOSYNTHESIS
COENZYME FAD BIOSYNTHESIS
FOLATE METABOLISM
GPI ANCHOR BIOSYNTHESIS
HEME METABOLISM
VITAMIN B6 METABOLISM
COENZYME NAD BIOSYNTHESIS
VIT
BLCA BRCA COAD ESCC HNSC KIRC LIHC LUAD LUSC OV PRAD SCLC STAD UCEC
Regulation Down Up
adj.P.Val 0.01 0.02 0.03 0.04
logFC −1.0 −0.5 0.0 0.5 1.0
adj.P.ValCutoff = 0.05, pAdjustMethod = BH
Glycosylation
FAD
B
Top disregulated tasks_Zhou2020
Conversion of asparate to asparagine
Glycine synthesis
Serine synthesis
Aspartate synthesis
Conversion of histidine to glutamate
Cysteine synthesis (need serine and methionine)
Homocysteine synthesis (need methionine)
Proline synthesis
AMI
CMP−N−acetylneuraminate synthesis
GDP−L−fucose synthesis
N−Acetylglucosamine synthesis
Synthesis of lactose
CAR
Biosynthesis of g3m8masn
Glucosaminyl−acylphosphatidylinositoll to deacylated−−
glycophosphatidylinositol (GPI)−anchored protein
GLY
Farnesyl−pyrophosphate synthesis
LIP
Guanosine triphosphate synthesis (GTP)
NUC
FAD synthesis
VIT
BLCA BRCA COAD HNSC KIRC LIHC LUAD LUSC OV PRAD SCLC STAD UCEC
Regulation Down Up
adj.P.Val 0.01 0.02 0.03
logFC −0.5 0.0 0.5 1.0 1.5
adj.P.ValCutoff = 0.05, pAdjustMethod = BH
C
Disregulated systems_Zhou2020
AMINO ACIDS METABOLISM
GLYCAN METABOLISM
LIPIDS METABOLISM
NUCLEOTIDE METABOLISM
VITAMIN & COFACTOR METABOLISM
CARBOHYDRATES METABOLISM
ENERGY METABOLISM
BLCA COAD ESCC HNSC KIRC LIHC LUAD LUSC OV PRAD SCLC STAD UCEC
Regulation Down Up
logFC −0.2 −0.1 0.0 0.1 0.2 0.3
adj.P.Val 0.01 0.02 0.03
adj.P.ValCutoff = 0.05, pAdjustMethod = BH

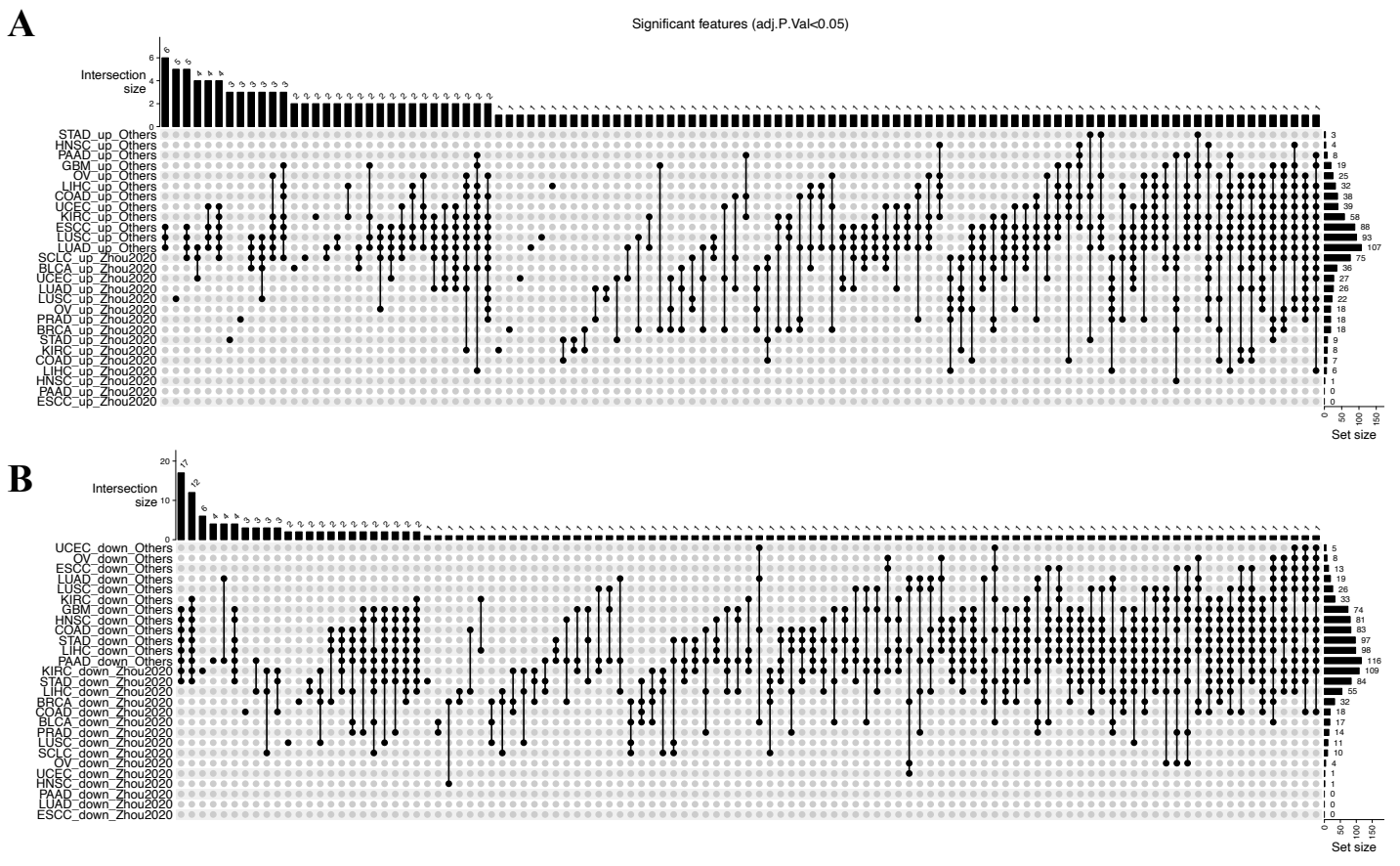
A
Significant features (adj.P.Val<0.05)
Intersection size
Set size
STAD_up_Others
HNSC_up_Others
PAAD_up_Others
GBM_up_Others
OV_up_Others
LIHC_up_Others
COAD_up_Others
UCEC_up_Others
KIRC_up_Others
ESCC_up_Others
LUSC_up_Others
LUAD_up_Others
SCLC_up_Zhou2020
BLCA_up_Zhou2020
UCEC_up_Zhou2020
LUAD_up_Zhou2020
LUSC_up_Zhou2020
OV_up_Zhou2020
PRAD_up_Zhou2020
BRCA_up_Zhou2020
STAD_up_Zhou2020
KIRC_up_Zhou2020
COAD_up_Zhou2020
LIHC_up_Zhou2020
HNSC_up_Zhou2020
PAAD_up_Zhou2020
ESCC_up_Zhou2020
B
Intersection size
Set size
UCEC_down_Others
OV_down_Others
ESCC_down_Others
LUAD_down_Others
LUSC_down_Others
KIRC_down_Others
GBM_down_Others
HNSC_down_Others
COAD_down_Others
STAD_down_Others
LIHC_down_Others
PAAD_down_Others
KIRC_down_Zhou2020
STAD_down_Zhou2020
LIHC_down_Zhou2020
BRCA_down_Zhou2020
COAD_down_Zhou2020
BLCA_down_Zhou2020
PRAD_down_Zhou2020
LUSC_down_Zhou2020
SCLC_down_Zhou2020
OV_down_Zhou2020
UCEC_down_Zhou2020
HNSC_down_Zhou2020
PAAD_down_Zhou2020
LUAD_down_Zhou2020
ESCC_down_Zhou2020

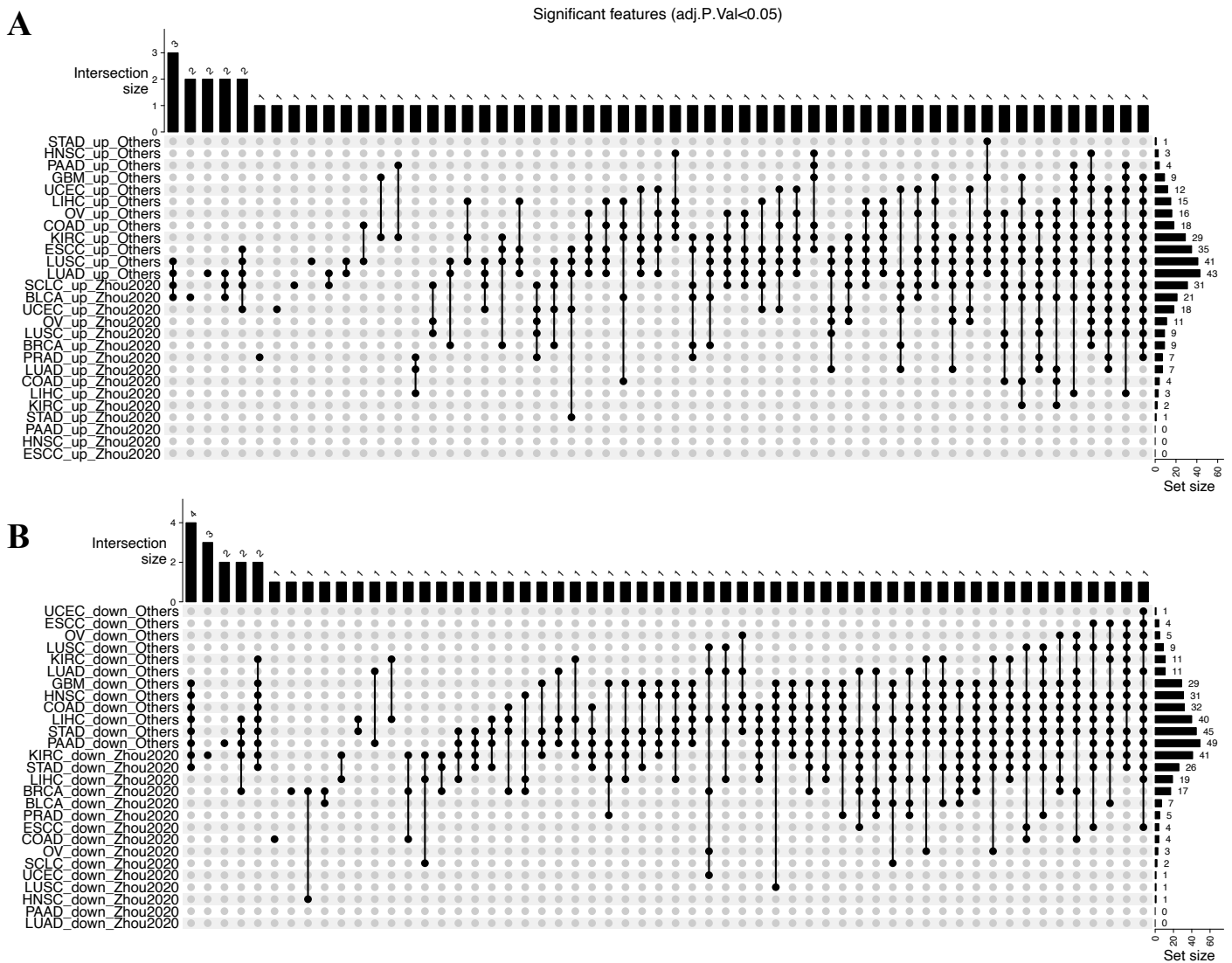
A
Significant features (adj.P.Val<0.05)
Intersection size
Set size
STAD_up_Others
HNSC_up_Others
PAAD_up_Others
GBM_up_Others
UCEC_up_Others
LIHC_up_Others
OV_up_Others
COAD_up_Others
KIRC_up_Others
ESCC_up_Others
LUSC_up_Others
LUAD_up_Others
SCLC_up_Zhou2020
BLCA_up_Zhou2020
UCEC_up_Zhou2020
OV_up_Zhou2020
LUSC_up_Zhou2020
BRCA_up_Zhou2020
PRAD_up_Zhou2020
LUAD_up_Zhou2020
COAD_up_Zhou2020
LIHC_up_Zhou2020
KIRC_up_Zhou2020
STAD_up_Zhou2020
PAAD_up_Zhou2020
HNSC_up_Zhou2020
ESCC_up_Zhou2020
B
Intersection size
Set size
UCEC_down_Others
ESCC_down_Others
OV_down_Others
LUSC_down_Others
KIRC_down_Others
LUAD_down_Others
GBM_down_Others
HNSC_down_Others
COAD_down_Others
LIHC_down_Others
STAD_down_Others
PAAD_down_Others
KIRC_down_Zhou2020
STAD_down_Zhou2020
LIHC_down_Zhou2020
BRCA_down_Zhou2020
BLCA_down_Zhou2020
PRAD_down_Zhou2020
ESCC_down_Zhou2020
COAD_down_Zhou2020
OV_down_Zhou2020
SCLC_down_Zhou2020
UCEC_down_Zhou2020
LUSC_down_Zhou2020
HNSC_down_Zhou2020
PAAD_down_Zhou2020
LUAD_down_Zhou2020

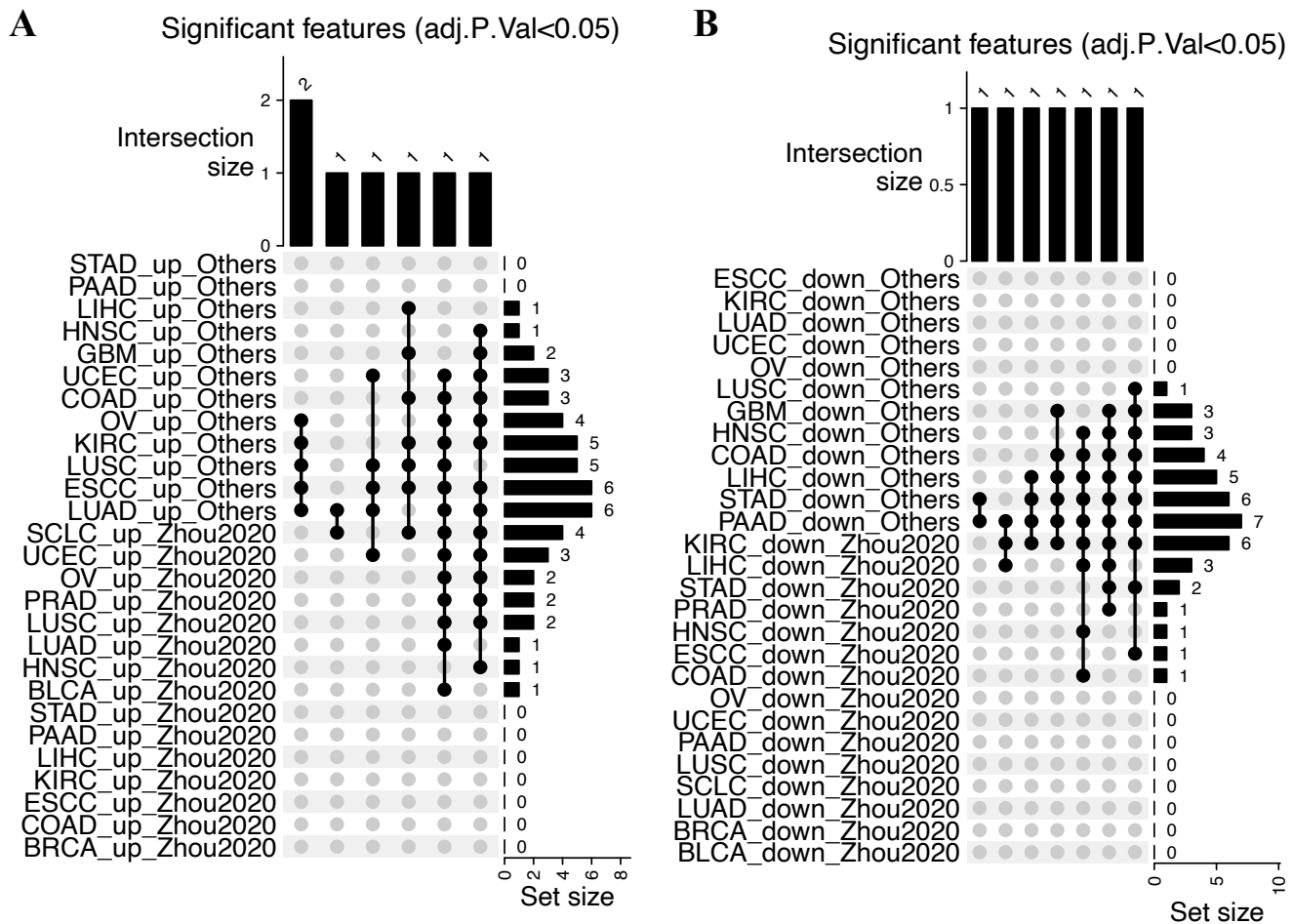
A
Significant features (adj.P.Val<0.05)
Intersection size
Set size
STAD_up_Others
PAAD_up_Others
LIHC_up_Others
HNSC_up_Others
GBM_up_Others
UCEC_up_Others
COAD_up_Others
OV_up_Others
KIRC_up_Others
LUSC_up_Others
ESCC_up_Others
LUAD_up_Others
SCLC_up_Zhou2020
UCEC_up_Zhou2020
OV_up_Zhou2020
PRAD_up_Zhou2020
LUSC_up_Zhou2020
LUAD_up_Zhou2020
HNSC_up_Zhou2020
BLCA_up_Zhou2020
STAD_up_Zhou2020
PAAD_up_Zhou2020
LIHC_up_Zhou2020
KIRC_up_Zhou2020
ESCC_up_Zhou2020
COAD_up_Zhou2020
BRCA_up_Zhou2020
B
Significant features (adj.P.Val<0.05)
Intersection size
Set size
ESCC_down_Others
KIRC_down_Others
LUAD_down_Others
UCEC_down_Others
OV_down_Others
LUSC_down_Others
GBM_down_Others
HNSC_down_Others
COAD_down_Others
LIHC_down_Others
STAD_down_Others
PAAD_down_Others
KIRC_down_Zhou2020
LIHC_down_Zhou2020
STAD_down_Zhou2020
PRAD_down_Zhou2020
HNSC_down_Zhou2020
ESCC_down_Zhou2020
COAD_down_Zhou2020
OV_down_Zhou2020
UCEC_down_Zhou2020
PAAD_down_Zhou2020
LUSC_down_Zhou2020
SCLC_down_Zhou2020
LUAD_down_Zhou2020
BRCA_down_Zhou2020
BLCA_down_Zhou2020

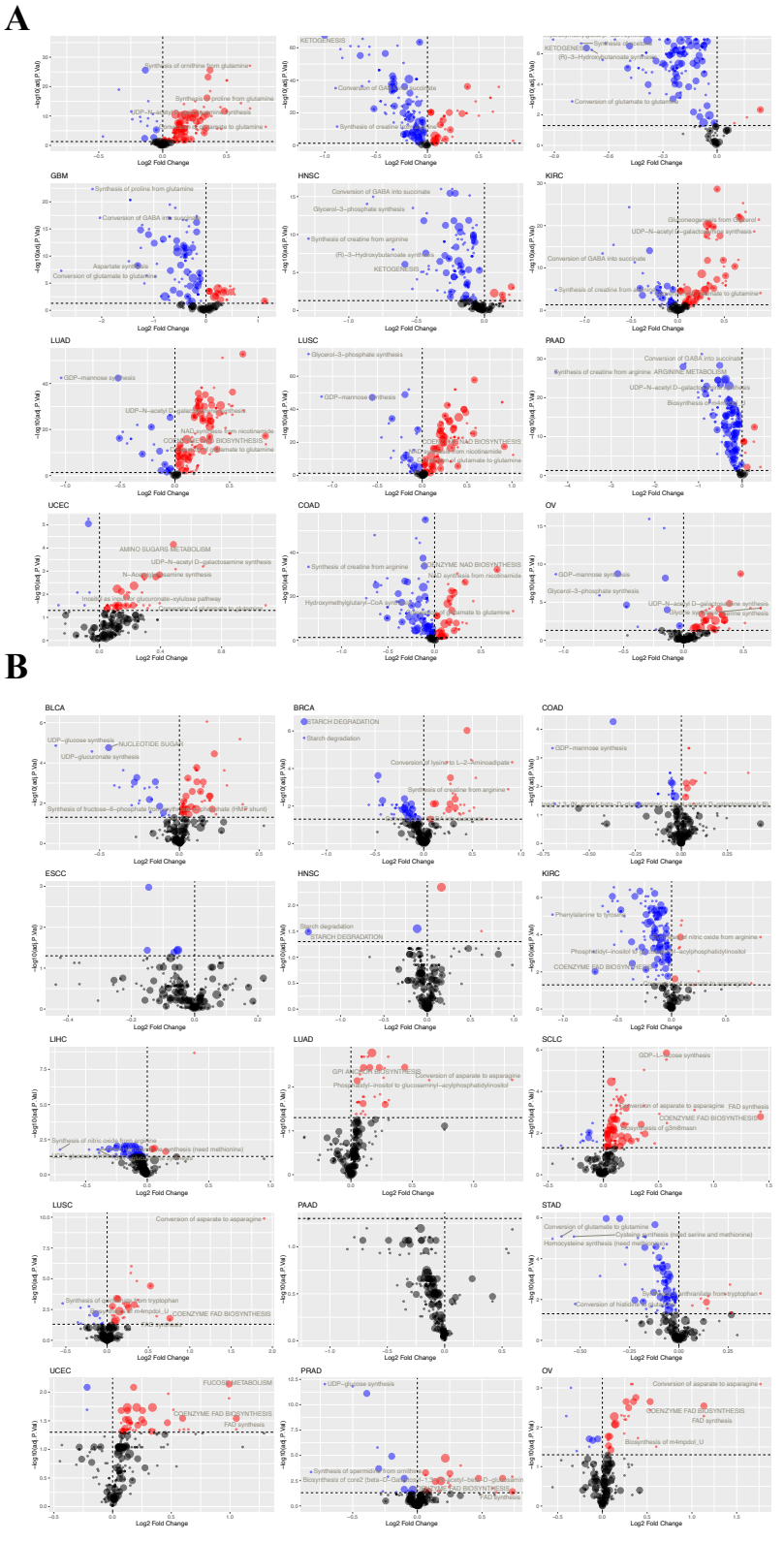
A
Synthesis of ornithine from glutamine
Synthesis of proline from glutamine
Log2 Fold Change
-log10(adj.P.Val)
KETOGENESIS
Conversion of GABA into succinate
Synthesis of creatine from arginine
(R)–3–Hydroxybutanoate synthesis
Conversion of glutamate to glutamine
GBM
Synthesis of proline from glutamine
Conversion of GABA into succinate
Aspartate synthesis
Conversion of glutamate to glutamine
HNSC
Conversion of GABA into succinate
Glycerol–3–phosphate synthesis
Synthesis of creatine from arginine
(R)–3–Hydroxybutanoate synthesis
KETOGENESIS
KIRC
Gluconeogenesis from Glycerol
UDP–N–acetyl D–galactosamine synthesis
Conversion of GABA into succinate
Synthesis of creatine from arginine
LUAD
GDP–mannose synthesis
UDP–N–acetyl D–galactosamine synthesis
NAD synthesis from nicotinamide
COENZYME NAD BIOSYNTHESIS
Conversion of glutamate to glutamine
LUSC
Glycerol–3–phosphate synthesis
GDP–mannose synthesis
COENZYME NAD BIOSYNTHESIS
NAD synthesis from nicotinamide
Conversion of glutamate to glutamine
PAAD
Conversion of GABA into succinate
Synthesis of creatine from arginine
ARGININE METABOLISM
UDP–N–acetyl D–galactosamine synthesis
Biosynthesis of
UCEC
AMINO SUGARS METABOLISM
UDP–N–acetyl D–galactosamine synthesis
N–acetylgalactosamine synthesis
Inositol phosphate metabolism
glucuronate–xylulose pathway
COAD
Synthesis of creatine from arginine
COENZYME NAD BIOSYNTHESIS
NAD synthesis from nicotinamide
Hydroxymethylglutaryl–CoA synthesis
Conversion of glutamate to glutamine
OV
GDP–mannose synthesis
Glycerol–3–phosphate synthesis
UDP–N–acetyl D–galactosamine synthesis
Biosynthesis of
B
BLCA
UDP–glucose synthesis
NUCLEOTIDE SUGARS
UDP–glucuronate synthesis
Synthesis of fructose–6–phosphate from glucose–6–phosphate (HMP shunt)
BRCA
STARCH DEGRADATION
Starch degradation
Conversion of lysine to L–2–Aminoadipate
Synthesis of creatine from arginine
COAD
GDP–mannose synthesis
ESCC
HNSC
Starch degradation
STARCH DEGRADATION
KIRC
Phenylalanine to tyrosine
Nitric oxide from arginine
Phosphatidyl–inositol of
–acylphosphatidylinositol
COENZYME FAD BIOSYNTHESIS
LIHC
Synthesis of nitric oxide from arginine
Synthesis (need methionine)
LUAD
GPI–anchor BIOSYNTHESIS
Conversion of asparate to asparagine
Phosphatidyl–inositol to glucosaminyl–acylphosphatidylinositol
SCLC
GDP–L–fucose synthesis
Conversion of asparate to asparagine
FAD synthesis
COENZYME FAD BIOSYNTHESIS
Biosynthesis of g3m8masn
LUSC
Conversion of asparate to asparagine
Synthesis of
from tryptophan
m4mpdol_U
COENZYME FAD BIOSYNTHESIS
PAAD
STAD
Conversion of glutamate to glutamine
Cysteine synthesis (need serine and methionine)
Homocysteine synthesis (need methionine)
Conversion of
from tryptophan
UCEC
FUCOSE METABOLISM
COENZYME FAD BIOSYNTHESIS
FAD synthesis
PRAD
UDP–glucose synthesis
Synthesis of spermidine from ornithine
Biosynthesis of core2 (beta–1,6–GlcNAc)
COENZYME FAD BIOSYNTHESIS
FAD synthesis
OV
Conversion of asparate to asparagine
COENZYME FAD BIOSYNTHESIS
FAD synthesis
Biosynthesis of m4mpdol_U

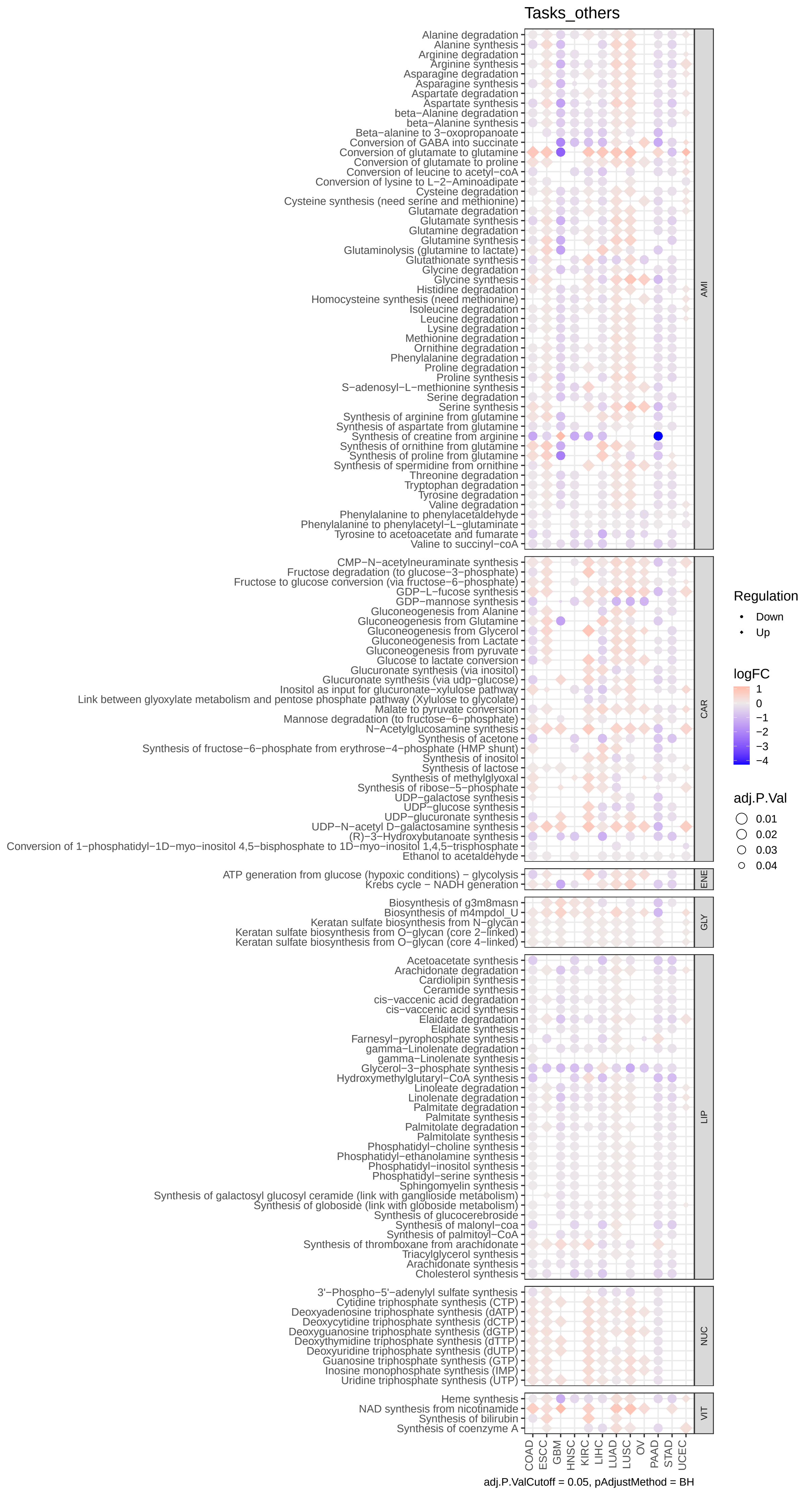
Tasks_others
Alanine degradation
Alanine synthesis
Arginine degradation
Arginine synthesis
Asparagine degradation
Asparagine synthesis
Aspartate degradation
Aspartate synthesis
beta−Alanine degradation
beta−Alanine synthesis
Beta−alanine to 3−oxopropanoate
Conversion of GABA into succinate
Conversion of glutamate to glutamine
Conversion of glutamate to proline
Conversion of leucine to acetyl−coA
Conversion of lysine to L−2−Aminoadipate
Cysteine degradation
Cysteine synthesis (need serine and methionine)
Glutamate degradation
Glutamate synthesis
Glutamine degradation
Glutamine synthesis
Glutaminolysis (glutamine to lactate)
Glutathionate synthesis
Glycine degradation
Glycine synthesis
Histidine degradation
Homocysteine synthesis (need methionine)
Isoleucine degradation
Leucine degradation
Lysine degradation
Methionine degradation
Ornithine degradation
Phenylalanine degradation
Proline degradation
Proline synthesis
S−adenosyl−L−methionine synthesis
Serine degradation
Serine synthesis
Synthesis of arginine from glutamine
Synthesis of aspartate from glutamine
Synthesis of creatine from arginine
Synthesis of ornithine from glutamine
Synthesis of proline from glutamine
Synthesis of spermidine from ornithine
Threonine degradation
Tryptophan degradation
Tyrosine degradation
Valine degradation
Phenylalanine to phenylacetaldehyde
Phenylalanine to phenylacetyl−L−glutaminate
Tyrosine to acetoacetate and fumarate
Valine to succinyl−coA
AMI
CMP−N−acetylneuraminate synthesis
Fructose degradation (to glucose−3−phosphate)
Fructose to glucose conversion (via fructose−6−phosphate)
GDP−L−fucose synthesis
GDP−mannose synthesis
Gluconeogenesis from Alanine
Gluconeogenesis from Glutamine
Gluconeogenesis from Glycerol
Gluconeogenesis from Lactate
Gluconeogenesis from pyruvate
Glucose to lactate conversion
Glucuronate synthesis (via inositol)
Glucuronate synthesis (via udp−glucose)
Inositol as input for glucuronate−xylulose pathway
Link between glyoxylate metabolism and pentose phosphate pathway (Xylulose to glycolate)
Malate to pyruvate conversion
Mannose degradation (to fructose−6−phosphate)
N−Acetylglucosamine synthesis
Synthesis of acetone
Synthesis of fructose−6−phosphate from erythrose−4−phosphate (HMP shunt)
Synthesis of inositol
Synthesis of lactose
Synthesis of methylglyoxal
Synthesis of ribose−5−phosphate
UDP−galactose synthesis
UDP−glucose synthesis
UDP−glucuronate synthesis
UDP−N−acetyl D−galactosamine synthesis
(R)−3−Hydroxybutanoate synthesis
Conversion of 1−phosphatidyl−1D−myo−inositol 4,5−bisphosphate to 1D−myo−inositol 1,4,5−trisphosphate
Ethanol to acetaldehyde
CAR
ATP generation from glucose (hypoxic conditions) − glycolysis
Krebs cycle − NADH generation
ENE
Biosynthesis of g3m8masn
Biosynthesis of m4mpdol_U
Keratan sulfate biosynthesis from N−glycan
Keratan sulfate biosynthesis from O−glycan (core 2−linked)
Keratan sulfate biosynthesis from O−glycan (core 4−linked)
GLY
Acetoacetate synthesis
Arachidonate degradation
Cardiolipin synthesis
Ceramide synthesis
cis−vaccenic acid degradation
cis−vaccenic acid synthesis
Elaidate degradation
Elaidate synthesis
Farnesyl−pyrophosphate synthesis
gamma−Linolenate degradation
gamma−Linolenate synthesis
Glycerol−3−phosphate synthesis
Hydroxymethylglutaryl−CoA synthesis
Linoleate degradation
Linolenate degradation
Palmitate degradation
Palmitate synthesis
Palmitolate degradation
Palmitolate synthesis
Phosphatidyl−choline synthesis
Phosphatidyl−ethanolamine synthesis
Phosphatidyl−inositol synthesis
Phosphatidyl−serine synthesis
Sphingomyelin synthesis
Synthesis of galactosyl glucosyl ceramide (link with ganglioside metabolism)
Synthesis of globoside (link with globoside metabolism)
Synthesis of glucocerebroside
Synthesis of malonyl−coa
Synthesis of palmitoyl−CoA
Synthesis of thromboxane from arachidonate
Triacylglycerol synthesis
Arachidonate synthesis
Cholesterol synthesis
LIP
3'−Phospho−5'−adenylyl sulfate synthesis
Cytidine triphosphate synthesis (CTP)
Deoxyadenosine triphosphate synthesis (dATP)
Deoxycytidine triphosphate synthesis (dCTP)
Deoxyguanosine triphosphate synthesis (dGTP)
Deoxythymidine triphosphate synthesis (dTTP)
Deoxyuridine triphosphate synthesis (dUTP)
Guanosine triphosphate synthesis (GTP)
Inosine monophosphate synthesis (IMP)
Uridine triphosphate synthesis (UTP)
NUC
Heme synthesis
NAD synthesis from nicotinamide
Synthesis of bilirubin
Synthesis of coenzyme A
VIT
COAD
ESCC
GBM
HNSC
KIRC
LIHC
LUAD
LUSC
OV
PAAD
STAD
UCEC
adj.P.ValCutoff = 0.05, pAdjustMethod = BH
Regulation
Down
Up
logFC
1
0
−1
−2
−3
−4
adj.P.Val
0.01
0.02
0.03
0.04

Tasks_Zhou2020
Alanine degradation
Alanine synthesis
Arginine degradation
Asparagine degradation
Asparagine synthesis
Aspartate degradation
Aspartate synthesis
beta−Alanine degradation
beta−Alanine synthesis
Beta−alanine to 3−oxopropanoate
Conversion of asparate to asparagine
Conversion of aspartate to arginine
Conversion of GABA into succinate
Conversion of histidine to histamine
Conversion of leucine to acetyl−coA
Conversion of lysine to L−2−Aminoadipate
Conversion of lysine to L−Saccharopine
Cysteine degradation
Glutamate degradation
Glutamate synthesis
Glutamine degradation
Glutamine synthesis
Glutathionate synthesis
Glycine synthesis
Homocysteine degradation
Isoleucine degradation
Leucine degradation
Lysine degradation
Ornithine degradation
Phenylalanine degradation
Phenylalanine to phenylacetaldehyde
Phenylalanine to phenylacetyl−L−glutaminate
Proline degradation
Serine synthesis
Synthesis of anthranilate from tryptophan
Synthesis of creatine from arginine
Synthesis of kynate from tryptophan
Synthesis of L−kynurenine from tryptophan
Synthesis of N−formylanthranilate from tryptophan
Synthesis of nitric oxide from arginine
Synthesis of proline from glutamine
Synthesis of quinolinate from tryptophan
Synthesis of serotonin from tryptophan
Threonine degradation
Tryptophan degradation
Tyrosine degradation
Tyrosine to acetoacetate and fumarate
Tyrosine to adrenaline
Tyrosine to dopamine
Valine degradation
Arginine synthesis
Conversion of aspartate to beta−alanine
Conversion of carnosine to beta−alanine
Conversion of glutamate to glutamine
Conversion of glutamate to proline
Conversion of glycine to pyruvate
Conversion of histidine to glutamate
Cysteine synthesis (need serine and methionine)
Glycine degradation
Histidine degradation
Homocysteine synthesis (need methionine)
Methionine degradation
Phenylalanine to tyrosine
Proline synthesis
S−adenosyl−L−methionine synthesis
Serine degradation
Synthesis of arginine from glutamine
Synthesis of aspartate from glutamine
Synthesis of ornithine from glutamine
Synthesis of spermidine from ornithine
Tyrosine synthesis (need phenylalanine)
Valine to succinyl−coA
AMI
CMP−N−acetylneuraminate synthesis
Fructose degradation (to glucose−3−phosphate)
Fructose to glucose conversion (via fructose−6−phosphate)
GDP−L−fucose synthesis
Gluconeogenesis from Alanine
Gluconeogenesis from Glutamine
Gluconeogenesis from Glycerol
Gluconeogenesis from Lactate
Gluconeogenesis from pyruvate
Glucose to lactate conversion
Inositol as input for glucuronate−xylulose pathway
Malate to pyruvate conversion
N−Acetylglucosamine synthesis
Starch degradation
Synthesis of fructose−6−phosphate from erythrose−4−phosphate (HMP shunt)
Synthesis of lactose
Synthesis of ribose−5−phosphate
UDP−galactose synthesis
UDP−N−acetyl D−galactosamine synthesis
(R)−3−Hydroxybutanoate synthesis
Conversion of 1−phosphatidyl−1D−myo−inositol 4,5−bisphosphate to 1D−myo−inositol 1,4,5−trisphosphate
Ethanol to acetaldehyde
GDP−mannose synthesis
Glucuronate synthesis (via inositol)
Glucuronate synthesis (via udp−glucose)
Mannose degradation (to fructose−6−phosphate)
Synthesis of acetone
Synthesis of inositol
Synthesis of methylglyoxal
UDP−glucose synthesis
UDP−glucuronate synthesis
CAR
ATP generation from glucose (hypoxic conditions) − glycolysis
Krebs cycle − NADH generation
Presence of the thioredoxin system through the thioredoxin reductase activity
Krebs cycle − oxidative decarboxylation of pyruvate
ENE
Biosynthesis of core2 (beta−D−Galactosyl−1,3−(N−acetyl−beta−D−glucosaminyl−1,6)−N−acetyl−D−galactosaminyl−R)
Biosynthesis of core4 (N−Acetyl−beta−D−glucosaminyl−1,6−(N−acetyl−beta−D−glucosaminyl−1,3)−N−acetyl−D−galactosaminyl−R)
Biosynthesis of g3m8masn
Biosynthesis of m4mpdol_U
Degradation of n2m2nmasn
Glucosaminyl−acylphosphatidylinositoll to deacylated−glycophosphatidylinositol (GPI)−anchored protein
Keratan sulfate biosynthesis from N−glycan
Keratan sulfate biosynthesis from O−glycan (core 2−linked)
Keratan sulfate biosynthesis from O−glycan (core 4−linked)
GLY
Acetoacetate synthesis
Arachidonate degradation
Arachidonate synthesis
Cardiolipin synthesis
Ceramide synthesis
Cholesterol synthesis
cis−vaccenic acid synthesis
Elaidate degradation
Elaidate synthesis
Farnesyl−pyrophosphate synthesis
gamma−Linolenate synthesis
Linolenate degradation
Palmitate synthesis
Palmitolate synthesis
Phosphatidyl−choline synthesis
Phosphatidyl−ethanolamine synthesis
Phosphatidyl−inositol synthesis
Phosphatidyl−serine synthesis
Sphingomyelin synthesis
Synthesis of galactosyl glucosyl ceramide (link with ganglioside metabolism)
Synthesis of globoside (link with globoside metabolism)
Synthesis of glucocerebroside
Synthesis of malonyl−coa
Synthesis of palmitoyl−CoA
Triacylglycerol synthesis
cis−vaccenic acid degradation
gamma−Linolenate degradation
Glycerol−3−phosphate synthesis
Hydroxymethylglutaryl−CoA synthesis
Linoleate degradation
Palmitate degradation
Palmitolate degradation
Synthesis of thromboxane from arachidonate
LIP
3'−Phospho−5'−adenylyl sulfate synthesis
AMP salvage from adenine
Cytidine triphosphate synthesis (CTP)
Degradation of cytosine
Degradation of uracil
Deoxyadenosine triphosphate synthesis (dATP)
Deoxycytidine triphosphate synthesis (dCTP)
Deoxyguanosine triphosphate synthesis (dGTP)
Deoxythymidine triphosphate synthesis (dTTP)
Guanosine triphosphate synthesis (GTP)
Inosine monophosphate synthesis (IMP)
Uridine triphosphate synthesis (UTP)
Degradation of adenine to urate
Degradation of guanine to urate
NUC
FAD synthesis
Phosphatidyl−inositol to glucosaminyl−acylphosphatidylinositol
Pyridoxal−phosphate synthesis
Synthesis of bilirubin
Synthesis of coenzyme A
Tetrahydrofolate synthesis
Heme synthesis
NAD synthesis from nicotinamide
VIT
BLCA
BRCA
COAD
HNSC
KIRC
LIHC
LUAD
LUSC
OV
PRAD
SCLC
STAD
UCEC
Regulation
Down
Up
adj.P.Val
0.01
0.02
0.03
0.04
logFC
−1
0
adj.P.ValCutoff = 0.05, pAdjustMethod = BH

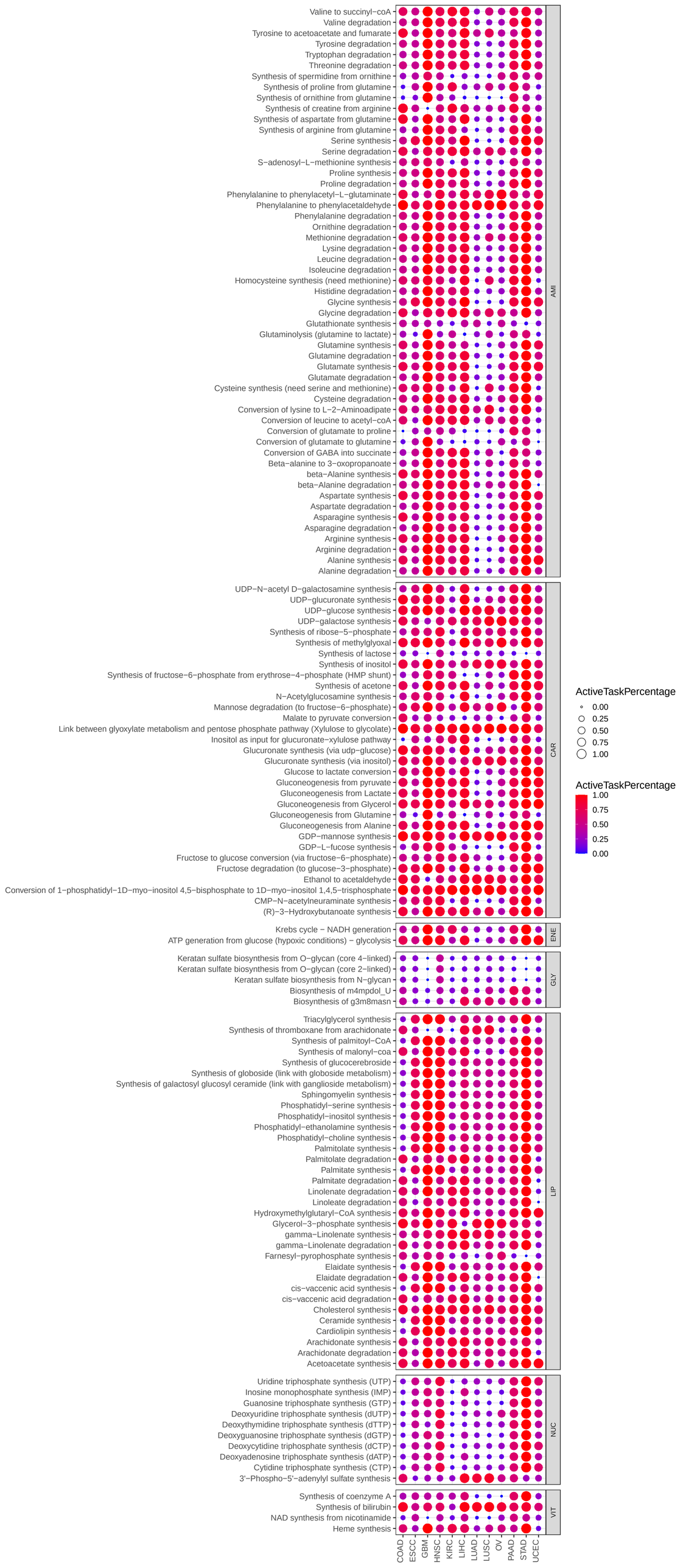
Valine to succinyl−coA
Valine degradation
Tyrosine to acetoacetate and fumarate
Tyrosine degradation
Tryptophan degradation
Threonine degradation
Synthesis of spermidine from ornithine
Synthesis of proline from glutamine
Synthesis of ornithine from glutamine
Synthesis of creatine from arginine
Synthesis of aspartate from glutamine
Synthesis of arginine from glutamine
Serine synthesis
Serine degradation
S−adenosyl−L−methionine synthesis
Proline synthesis
Proline degradation
Phenylalanine to phenylacetyl−L−glutaminate
Phenylalanine to phenylacetaldehyde
Phenylalanine degradation
Ornithine degradation
Methionine degradation
Lysine degradation
Leucine degradation
Isoleucine degradation
Homocysteine synthesis (need methionine)
Histidine degradation
Glycine synthesis
Glycine degradation
Glutathionate synthesis
Glutaminolysis (glutamine to lactate)
Glutamine synthesis
Glutamine degradation
Glutamate synthesis
Glutamate degradation
Cysteine synthesis (need serine and methionine)
Cysteine degradation
Conversion of lysine to L−2−Aminoadipate
Conversion of leucine to acetyl−coA
Conversion of glutamate to proline
Conversion of glutamate to glutamine
Conversion of GABA into succinate
Beta−alanine to 3−oxopropanoate
beta−Alanine synthesis
beta−Alanine degradation
Aspartate synthesis
Aspartate degradation
Asparagine synthesis
Asparagine degradation
Arginine synthesis
Arginine degradation
Alanine synthesis
Alanine degradation
AMI
UDP−N−acetyl D−galactosamine synthesis
UDP−glucuronate synthesis
UDP−glucose synthesis
UDP−galactose synthesis
Synthesis of ribose−5−phosphate
Synthesis of methylglyoxal
Synthesis of lactose
Synthesis of inositol
Synthesis of fructose−6−phosphate from erythrose−4−phosphate (HMP shunt)
Synthesis of acetone
N−Acetylglucosamine synthesis
Mannose degradation (to fructose−6−phosphate)
Malate to pyruvate conversion
Link between glyoxylate metabolism and pentose phosphate pathway (Xylulose to glycolate)
Inositol as input for glucuronate−xylulose pathway
Glucuronate synthesis (via udp−glucose)
Glucuronate synthesis (via inositol)
Glucose to lactate conversion
Gluconeogenesis from pyruvate
Gluconeogenesis from Lactate
Gluconeogenesis from Glycerol
Gluconeogenesis from Glutamine
Gluconeogenesis from Alanine
GDP−mannose synthesis
GDP−L−fucose synthesis
Fructose to glucose conversion (via fructose−6−phosphate)
Fructose degradation (to glucose−3−phosphate)
Ethanol to acetaldehyde
Conversion of 1−phosphatidyl−1D−myo−inositol 4,5−bisphosphate to 1D−myo−inositol 1,4,5−trisphosphate
CMP−N−acetylneuraminate synthesis
(R)−3−Hydroxybutanoate synthesis
CAR
Krebs cycle − NADH generation
ATP generation from glucose (hypoxic conditions) − glycolysis
ENE
Keratan sulfate biosynthesis from O−glycan (core 4−linked)
Keratan sulfate biosynthesis from O−glycan (core 2−linked)
Keratan sulfate biosynthesis from N−glycan
Biosynthesis of m4mpdol_U
Biosynthesis of g3m8masn
GLY
Triacylglycerol synthesis
Synthesis of thromboxane from arachidonate
Synthesis of palmitoyl−CoA
Synthesis of malonyl−coa
Synthesis of glucocerebroside
Synthesis of globoside (link with globoside metabolism)
Synthesis of galactosyl glucosyl ceramide (link with ganglioside metabolism)
Sphingomyelin synthesis
Phosphatidyl−serine synthesis
Phosphatidyl−inositol synthesis
Phosphatidyl−ethanolamine synthesis
Phosphatidyl−choline synthesis
Palmitolate synthesis
Palmitolate degradation
Palmitate synthesis
Palmitate degradation
Linolenate degradation
Linoleate degradation
Hydroxymethylglutaryl−CoA synthesis
Glycerol−3−phosphate synthesis
gamma−Linolenate synthesis
gamma−Linolenate degradation
Farnesyl−pyrophosphate synthesis
Elaidate synthesis
Elaidate degradation
cis−vaccenic acid synthesis
cis−vaccenic acid degradation
Cholesterol synthesis
Ceramide synthesis
Cardiolipin synthesis
Arachidonate synthesis
Arachidonate degradation
Acetoacetate synthesis
LIP
Uridine triphosphate synthesis (UTP)
Inosine monophosphate synthesis (IMP)
Guanosine triphosphate synthesis (GTP)
Deoxyuridine triphosphate synthesis (dUTP)
Deoxythymidine triphosphate synthesis (dTTP)
Deoxyguanosine triphosphate synthesis (dGTP)
Deoxycytidine triphosphate synthesis (dCTP)
Deoxyadenosine triphosphate synthesis (dATP)
Cytidine triphosphate synthesis (CTP)
3'−Phospho−5'−adenylyl sulfate synthesis
NUC
Synthesis of coenzyme A
Synthesis of bilirubin
NAD synthesis from nicotinamide
Heme synthesis
VIT
COAD
ESCC
GBM
HNSC
KIRC
LIHC
LUAD
LUSC
OV
PAAD
STAD
UCEC
ActiveTaskPercentage
0.00
0.25
0.50
0.75
1.00
ActiveTaskPercentage
1.00
0.75
0.50
0.25
0.00

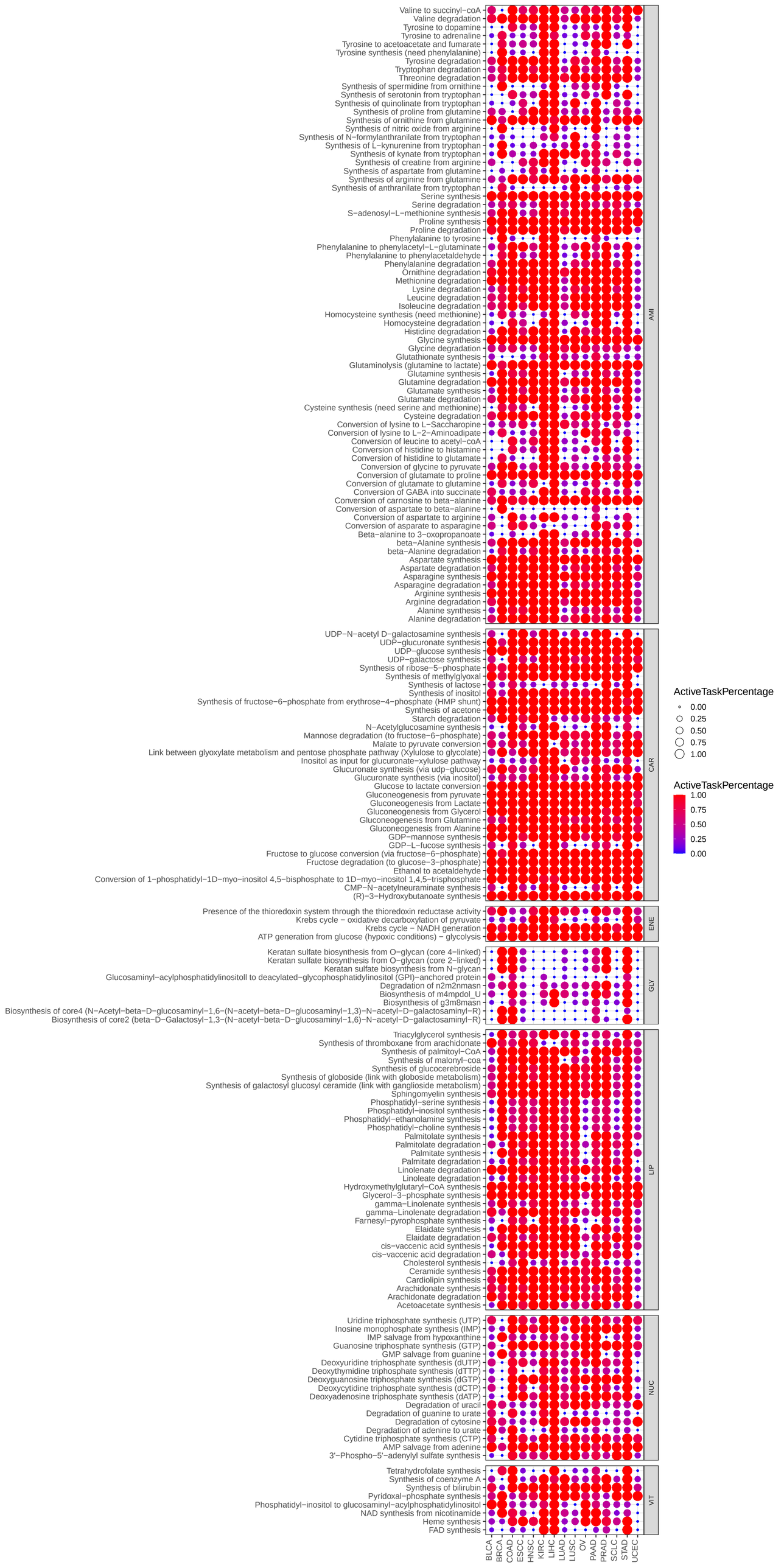
Valine to succinyl−coA
Valine degradation
Tyrosine to dopamine
Tyrosine to adrenaline
Tyrosine to acetoacetate and fumarate
Tyrosine synthesis (need phenylalanine)
Tyrosine degradation
Tryptophan degradation
Threonine degradation
Synthesis of spermidine from ornithine
Synthesis of serotonin from tryptophan
Synthesis of quinolinate from tryptophan
Synthesis of proline from glutamine
Synthesis of ornithine from glutamine
Synthesis of nitric oxide from arginine
Synthesis of N−formylanthranilate from tryptophan
Synthesis of L−kynurenine from tryptophan
Synthesis of kynate from tryptophan
Synthesis of creatine from arginine
Synthesis of aspartate from glutamine
Synthesis of arginine from glutamine
Synthesis of anthranilate from tryptophan
Serine synthesis
Serine degradation
S−adenosyl−L−methionine synthesis
Proline synthesis
Proline degradation
Phenylalanine to tyrosine
Phenylalanine to phenylacetyl−L−glutaminate
Phenylalanine to phenylacetaldehyde
Phenylalanine degradation
Ornithine degradation
Methionine degradation
Lysine degradation
Leucine degradation
Isoleucine degradation
Homocysteine synthesis (need methionine)
Homocysteine degradation
Histidine degradation
Glycine synthesis
Glycine degradation
Glutathionate synthesis
Glutaminolysis (glutamine to lactate)
Glutamine synthesis
Glutamine degradation
Glutamate synthesis
Glutamate degradation
Cysteine synthesis (need serine and methionine)
Cysteine degradation
Conversion of lysine to L−Saccharopine
Conversion of lysine to L−2−Aminoadipate
Conversion of leucine to acetyl−coA
Conversion of histidine to histamine
Conversion of histidine to glutamate
Conversion of glycine to pyruvate
Conversion of glutamate to proline
Conversion of glutamate to glutamine
Conversion of GABA into succinate
Conversion of carnosine to beta−alanine
Conversion of aspartate to beta−alanine
Conversion of aspartate to arginine
Conversion of asparate to asparagine
Beta−alanine to 3−oxopropanoate
beta−Alanine synthesis
beta−Alanine degradation
Aspartate synthesis
Aspartate degradation
Asparagine synthesis
Asparagine degradation
Arginine synthesis
Arginine degradation
Alanine synthesis
Alanine degradation
AMI
UDP−N−acetyl D−galactosamine synthesis
UDP−glucuronate synthesis
UDP−glucose synthesis
UDP−galactose synthesis
Synthesis of ribose−5−phosphate
Synthesis of methylglyoxal
Synthesis of lactose
Synthesis of inositol
Synthesis of fructose−6−phosphate from erythrose−4−phosphate (HMP shunt)
Synthesis of acetone
Starch degradation
N−Acetylglucosamine synthesis
Mannose degradation (to fructose−6−phosphate)
Malate to pyruvate conversion
Link between glyoxylate metabolism and pentose phosphate pathway (Xylulose to glycolate)
Inositol as input for glucuronate−xylulose pathway
Glucuronate synthesis (via udp−glucose)
Glucuronate synthesis (via inositol)
Glucose to lactate conversion
Gluconeogenesis from pyruvate
Gluconeogenesis from Lactate
Gluconeogenesis from Glycerol
Gluconeogenesis from Glutamine
Gluconeogenesis from Alanine
GDP−mannose synthesis
GDP−L−fucose synthesis
Fructose to glucose conversion (via fructose−6−phosphate)
Fructose degradation (to glucose−3−phosphate)
Ethanol to acetaldehyde
Conversion of 1−phosphatidyl−1D−myo−inositol 4,5−bisphosphate to 1D−myo−inositol 1,4,5−trisphosphate
CMP−N−acetylneuraminate synthesis
(R)−3−Hydroxybutanoate synthesis
CAR
Presence of the thioredoxin system through the thioredoxin reductase activity
Krebs cycle − oxidative decarboxylation of pyruvate
Krebs cycle − NADH generation
ATP generation from glucose (hypoxic conditions) − glycolysis
ENE
Keratan sulfate biosynthesis from O−glycan (core 4−linked)
Keratan sulfate biosynthesis from O−glycan (core 2−linked)
Keratan sulfate biosynthesis from N−glycan
Glucosaminyl−acylphosphatidylinositoll to deacylated−glycophosphatidylinositol (GPI)−anchored protein
Degradation of n2m2nmasn
Biosynthesis of m4mpdol_U
Biosynthesis of g3m8masn
Biosynthesis of core4 (N−Acetyl−beta−D−glucosaminyl−1,6−(N−acetyl−beta−D−glucosaminyl−1,3)−N−acetyl−D−galactosaminyl−R)
Biosynthesis of core2 (beta−D−Galactosyl−1,3−(N−acetyl−beta−D−glucosaminyl−1,6)−N−acetyl−D−galactosaminyl−R)
GLY
Triacylglycerol synthesis
Synthesis of thromboxane from arachidonate
Synthesis of palmitoyl−CoA
Synthesis of malonyl−coa
Synthesis of glucocerebroside
Synthesis of globoside (link with globoside metabolism)
Synthesis of galactosyl glucosyl ceramide (link with ganglioside metabolism)
Sphingomyelin synthesis
Phosphatidyl−serine synthesis
Phosphatidyl−inositol synthesis
Phosphatidyl−ethanolamine synthesis
Phosphatidyl−choline synthesis
Palmitolate synthesis
Palmitolate degradation
Palmitate synthesis
Palmitate degradation
Linolenate degradation
Linoleate degradation
Hydroxymethylglutaryl−CoA synthesis
Glycerol−3−phosphate synthesis
gamma−Linolenate synthesis
gamma−Linolenate degradation
Farnesyl−pyrophosphate synthesis
Elaidate synthesis
Elaidate degradation
cis−vaccenic acid synthesis
cis−vaccenic acid degradation
Cholesterol synthesis
Ceramide synthesis
Cardiolipin synthesis
Arachidonate synthesis
Arachidonate degradation
Acetoacetate synthesis
LIP
Uridine triphosphate synthesis (UTP)
Inosine monophosphate synthesis (IMP)
IMP salvage from hypoxanthine
Guanosine triphosphate synthesis (GTP)
GMP salvage from guanine
Deoxyuridine triphosphate synthesis (dUTP)
Deoxythymidine triphosphate synthesis (dTTP)
Deoxyguanosine triphosphate synthesis (dGTP)
Deoxycytidine triphosphate synthesis (dCTP)
Deoxyadenosine triphosphate synthesis (dATP)
Degradation of uracil
Degradation of guanine to urate
Degradation of cytosine
Degradation of adenine to urate
Cytidine triphosphate synthesis (CTP)
AMP salvage from adenine
3'−Phospho−5'−adenylyl sulfate synthesis
NUC
Tetrahydrofolate synthesis
Synthesis of coenzyme A
Synthesis of bilirubin
Pyridoxal−phosphate synthesis
Phosphatidyl−inositol to glucosaminyl−acylphosphatidylinositol
NAD synthesis from nicotinamide
Heme synthesis
FAD synthesis
VIT
BLCA
BRCA
COAD
ESCC
HNSC
KIRC
LIHC
LUAD
LUSC
OV
PAAD
PRAD
SCLC
STAD
UCEC
ActiveTaskPercentage
0.00
0.25
0.50
0.75
1.00
ActiveTaskPercentage
1.00
0.75
0.50
0.25
0.00

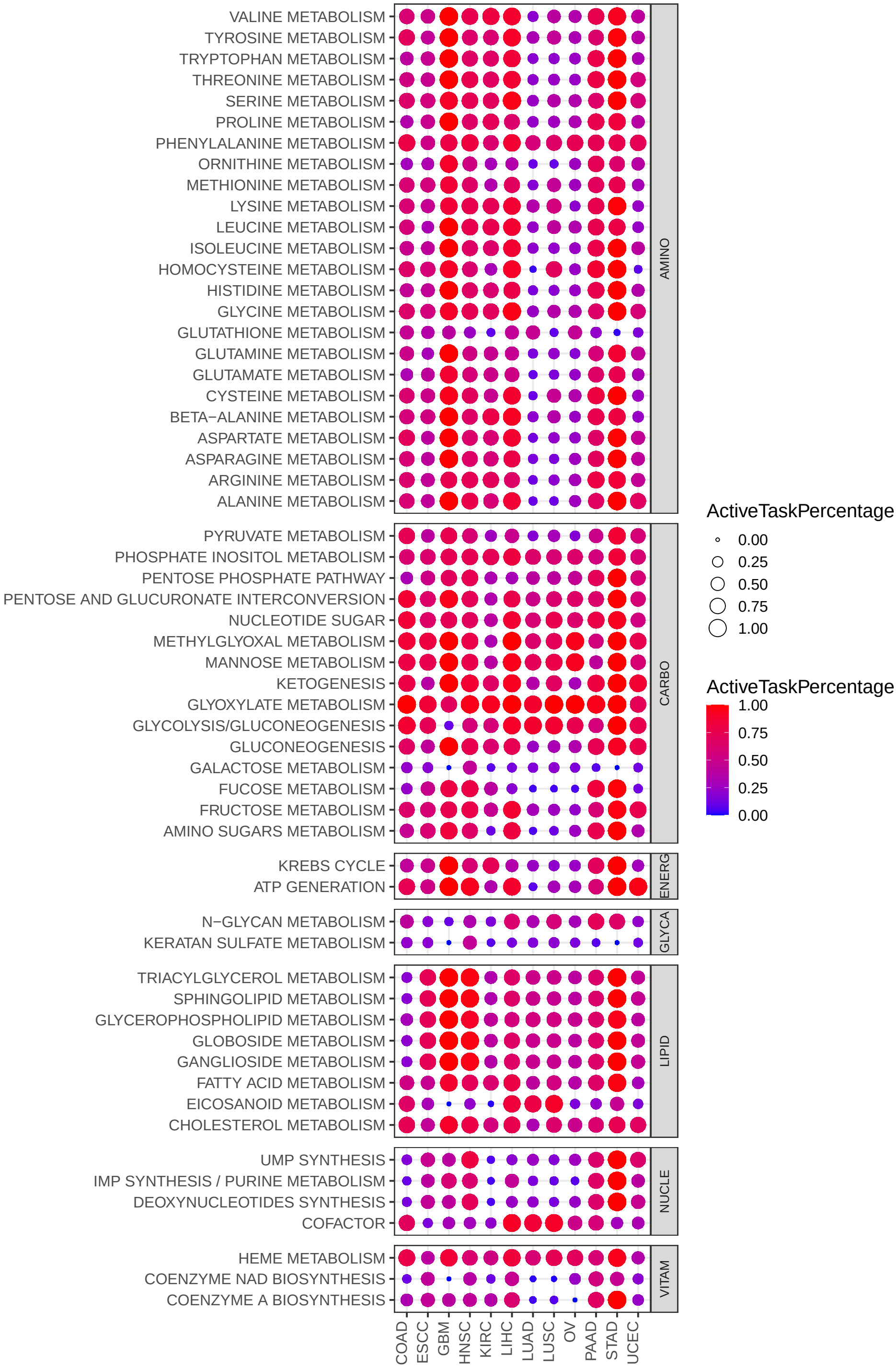
VALINE METABOLISM
TYROSINE METABOLISM
TRYPTOPHAN METABOLISM
THREONINE METABOLISM
SERINE METABOLISM
PROLINE METABOLISM
PHENYLALANINE METABOLISM
ORNITHINE METABOLISM
METHIONINE METABOLISM
LYSINE METABOLISM
LEUCINE METABOLISM
ISOLEUCINE METABOLISM
HOMOCYSTEINE METABOLISM
HISTIDINE METABOLISM
GLYCINE METABOLISM
GLUTATHIONE METABOLISM
GLUTAMINE METABOLISM
GLUTAMATE METABOLISM
CYSTEINE METABOLISM
BETA−ALANINE METABOLISM
ASPARTATE METABOLISM
ASPARAGINE METABOLISM
ARGININE METABOLISM
ALANINE METABOLISM
AMINO
PYRUVATE METABOLISM
PHOSPHATE INOSITOL METABOLISM
PENTOSE PHOSPHATE PATHWAY
PENTOSE AND GLUCURONATE INTERCONVERSION
NUCLEOTIDE SUGAR
METHYLGLYOXAL METABOLISM
MANNOSE METABOLISM
KETOGENESIS
GLYOXYLATE METABOLISM
GLYCOLYSIS/GLUCONEOGENESIS
GLUCONEOGENESIS
GALACTOSE METABOLISM
FUCOSE METABOLISM
FRUCTOSE METABOLISM
AMINO SUGARS METABOLISM
CARBO
KREBS CYCLE
ATP GENERATION
ENERG
N−GLYCAN METABOLISM
KERATAN SULFATE METABOLISM
GLYCA
TRIACYLGLYCEROL METABOLISM
SPHINGOLIPID METABOLISM
GLYCEROPHOSPHOLIPID METABOLISM
GLOBOSIDE METABOLISM
GANGLIOSIDE METABOLISM
FATTY ACID METABOLISM
EICOSANOID METABOLISM
CHOLESTEROL METABOLISM
LIPID
UMP SYNTHESIS
IMP SYNTHESIS / PURINE METABOLISM
DEOXYNUCLEOTIDES SYNTHESIS
COFACTOR
NUCLE
HEME METABOLISM
COENZYME NAD BIOSYNTHESIS
COENZYME A BIOSYNTHESIS
VITAM
COAD
ESCC
GBM
HNSC
KIRC
LIHC
LUAD
LUSC
OV
PAAD
STAD
UCEC
ActiveTaskPercentage
0.00
0.25
0.50
0.75
1.00
ActiveTaskPercentage
1.00
0.75
0.50
0.25
0.00

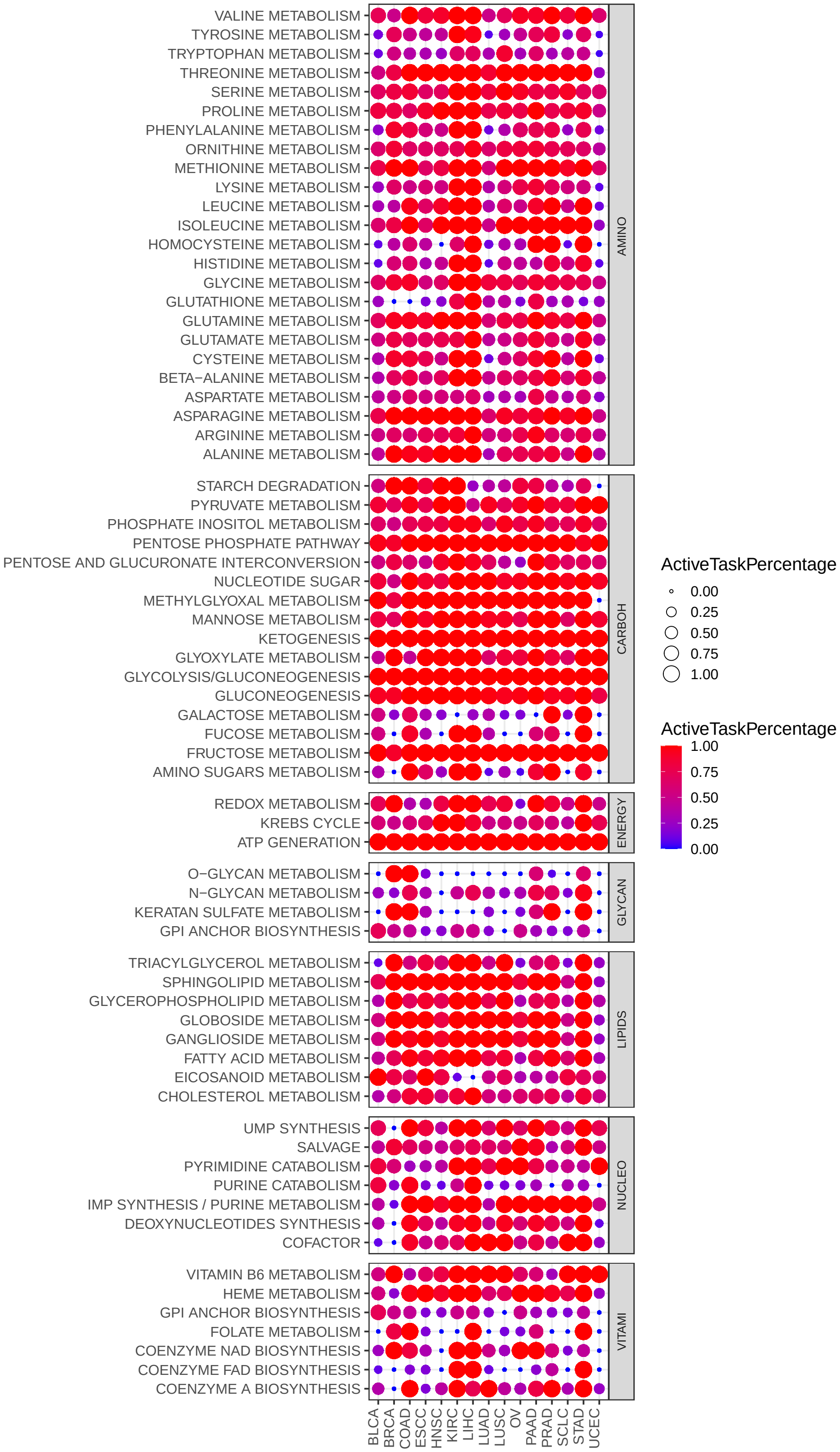
VALINE METABOLISM
TYROSINE METABOLISM
TRYPTOPHAN METABOLISM
THREONINE METABOLISM
SERINE METABOLISM
PROLINE METABOLISM
PHENYLALANINE METABOLISM
ORNITHINE METABOLISM
METHIONINE METABOLISM
LYSINE METABOLISM
LEUCINE METABOLISM
ISOLEUCINE METABOLISM
HOMOCYSTEINE METABOLISM
HISTIDINE METABOLISM
GLYCINE METABOLISM
GLUTATHIONE METABOLISM
GLUTAMINE METABOLISM
GLUTAMATE METABOLISM
CYSTEINE METABOLISM
BETA−ALANINE METABOLISM
ASPARTATE METABOLISM
ASPARAGINE METABOLISM
ARGININE METABOLISM
ALANINE METABOLISM
AMINO
STARCH DEGRADATION
PYRUVATE METABOLISM
PHOSPHATE INOSITOL METABOLISM
PENTOSE PHOSPHATE PATHWAY
PENTOSE AND GLUCURONATE INTERCONVERSION
NUCLEOTIDE SUGAR
METHYLGLYOXAL METABOLISM
MANNOSE METABOLISM
KETOGENESIS
GLYOXYLATE METABOLISM
GLYCOLYSIS/GLUCONEOGENESIS
GLUCONEOGENESIS
GALACTOSE METABOLISM
FUCOSE METABOLISM
FRUCTOSE METABOLISM
AMINO SUGARS METABOLISM
CARBOH
REDOX METABOLISM
KREBS CYCLE
ATP GENERATION
ENERGY
O−GLYCAN METABOLISM
N−GLYCAN METABOLISM
KERATAN SULFATE METABOLISM
GPI ANCHOR BIOSYNTHESIS
GLYCAN
TRIACYLGLYCEROL METABOLISM
SPHINGOLIPID METABOLISM
GLYCEROPHOSPHOLIPID METABOLISM
GLOBOSIDE METABOLISM
GANGLIOSIDE METABOLISM
FATTY ACID METABOLISM
EICOSANOID METABOLISM
CHOLESTEROL METABOLISM
LIPIDS
UMP SYNTHESIS
SALVAGE
PYRIMIDINE CATABOLISM
PURINE CATABOLISM
IMP SYNTHESIS / PURINE METABOLISM
DEOXYNUCLEOTIDES SYNTHESIS
COFACTOR
NUCLEO
VITAMIN B6 METABOLISM
HEME METABOLISM
GPI ANCHOR BIOSYNTHESIS
FOLATE METABOLISM
COENZYME NAD BIOSYNTHESIS
COENZYME FAD BIOSYNTHESIS
COENZYME A BIOSYNTHESIS
VITAMI
BLCA
BRCA
COAD
ESCC
HNSC
KIRC
LIHC
LUAD
LUSC
OV
PAAD
PRAD
SCLC
STAD
UCEC
ActiveTaskPercentage
0.00
0.25
0.50
0.75
1.00
ActiveTaskPercentage
1.00
0.75
0.50
0.25
0.00